AN ABSTRACT OF THE THESIS OF

Benjamin J. Norris for the degree of Master of Science in Electrical and Computer Engineering presented on June 11, 1999.

Title: Characterization of Organic Light-Emitting Devices

Redacted for Privacy

Abstract approved.

John F. Wager

In this thesis steady-state (*i.e.* steady-state with respect to the applied voltage waveform) transient current-transient voltage [i(t)-v(t)], transient brightness-transient current [b(t)-i(t)], transient brightness-transient voltage [b(t)-v(t)], transient current [i(t)], transient brightness [b(t)], and detrapped charge analysis are introduced as novel organic light emitting device (OLED) characterization methods. These analysis methods involve measurement of the instantaneous voltage [v(t)] across, the instantaneous current [i(t)] through, and the instantaneous brightness [b(t)] from an OLED when it is subjected to a bipolar, piecewise-linear applied voltage waveform. The utility of these characterization methods is demonstrated via comparison of different types of OLEDs and polymer light emitting devices (PLEDs) and from a preliminary study of OLED aging. Some of the device parameters obtained from these characterization methods include: OLED capacitance, accumulated charge, electron transport layer (ETL) thickness, hole transport layer (HTL) thickness, OLED thickness, parallel resistance, and series resistance. A current bump observed in i(t)-v(t) curves is attributed to the removal of accumulated hole charge from the ETL/HTL interface and is only observed in heterojunctions (*i.e.* OLEDs), not in single-layer devices (*i.e.* PLEDs). Using the characterization methods developed in this thesis, two important OLED device physics conclusions are obtained: (1) Hole accumulation at the ETL/HTL interface plays an important role in establishing balanced charge injection of electrons and holes into the OLED. (2) The ETL

behaves as a leaky insulator while the HTL more efficiently conducts charge and acts as a voltage-dependent resistor.

A preliminary investigation of the aging properties of OLEDs is presented as further evidence of the utility of the novel characterization methods developed in this thesis. In general, aging is characterized by a softer turn on of the forward bias portions of i(t)-v(t) and b(t)-v(t) curves. Also, some aging recovery is possible if the OLEDs are subjected to a zero or reverse bias.

©Copyright by Benjamin J. Norris

June 11, 1999

All Rights Reserved

Characterization of Organic Light-Emitting Devices

by

Benjamin J. Norris

A THESIS

submitted to

Oregon State University

in partial fulfillment of the

requirements for the degree of

Master of Science

Completed June 11, 1999

Commencement June 2000

Master of Science thesis of Benjamin J. Norris presented on June 11, 1999

APPROVED:

Redacted for Privacy

Major Professor, representing Electrical and Computer Engineering

Redacted for Privacy

Head of Department of Electrical and Computer Engineering

Redacted for Privacy

Dean of Graduate School

I understand that my thesis will become part of the permanent collection of Oregon State University libraries. My signature below authorizes release of my thesis to any reader upon request.

Redacted for Privacy

Benjamin J. Norris, Author

ACKNOWLEDGEMENTS

First, I would like to thank my wife, Catherine, for her support and understanding throughout the research and writing of this thesis. Also, I would like to thank my mother and father who have and encouraged and supported me throughout the course of my education. I would like to thank Dr. John Wager for his guidance and support. His door is always open and his enthusiasm for teaching and research is unmatched. I would also like to thank my committee for taking the time to review my thesis. Finally, I wish to thank Pat Green and Bill Barrow for helpful discussions and Ching Tang and Yang Yang for providing OLEDs. This work was supported by the U.S. Army Research Office under Contract No. DAAG55-9710226.

TABLE OF CONTENTS

TABLE OF CONTENTS (CONTINUED)

TABLE OF CONTENTS (CONTINUED)

LIST OF FIGURES

LIST OF FIGURES (CONTINUED)

LIST OF FIGURES (CONTINUED)

LIST OF FIGURES (CONTINUED)

LIST OF TABLES

Chapter 1
Introduction

Organic materials have been suggested for application in many fields traditionally dominated by inorganic semiconductors. The major advantage of organic materials is that they can be deposited by evaporation and spin-coating. These deposition methods are less costly and simpler than most of the deposition methods required for inorganic semiconductors. In addition, the vast array of organic materials offers an untapped source of possible material properties useful in semiconductor-based industries. Although organic materials possess properties that are advantageous to the integrated circuit industry, they are perhaps best suited to the display industry. Many organic materials have a high fluorescence quantum efficiency in the visible spectrum. Efficient organic phosphors are available in red, green, and blue, making an organic based full-color display possible. One of the largest barriers to the commercial realization of organic-based displays is the lack of understanding of the physics of their operation.

The organic light emitting device (OLED) proposed by C. W. Tang and S. A. VanSlyke possess many of the characteristics required for use in a display. [1, 2] It requires a low driving voltage (<10 V), possesses a high external quantum efficiency (1%), high luminous efficiency (1.5 lm/W), and high brightness (> 1000 cd/m^2). However, the aging characteristics are poor and the physics of operation of these devices are poorly understood. The OLED proposed by Tang and VanSlyke is a dual layer device with one layer predominately transporting holes (HTL) and the other electrons (ETL). [1, 2] The electrons and holes are thought to recombine near the junction via Frenkel excitons. In addition to the small-molecule dual-layer device, proposed by Tang and VanSlyke, devices possessing a recombination layer between the HTL and ETL, and polymer-based devices have been suggested.

OLEDs offer unique possibilities compared to other display technologies. The organic layers can be deposited on a wide range of substrates including flexible plastic, making roll-to-roll processing possible. This, combined with the fact that the absorption band of many organic molecules is shifted from that of the luminescence band makes large-area, flexible, transparent displays possible. A flexible, transparent display could be hung almost anywhere; for example, on a car or airplane windshield. The relative expense of some OLEDs may be so low that greeting cards with messages displayed in OLEDs are a possibility. In recent years, there has been a strong interest in making displays lighter and brighter with a large viewing angle. Like all electroluminescent devices, OLEDs have a wide viewing angle compared to liquid-crystal displays (LCDs) and are much less bulky than a cathode ray tube (CRT). Poor aging characteristics may prevent OLEDs from challenging high-end displays such as CRTs and LCDs, but for low-end technologies, like automotive displays and cellular phones, OLED-based displays may prevail. If they can be constructed very inexpensively, they may even challenge CRTs and LCDs as disposable displays. Clearly, there are many advantages to OLED technology. However, the aging characteristics and current transport properties must be understood before practical OLED displays are commercially viable.

The DC current transport characteristics of OLEDs are a topic of current research, but little work has been done with AC characterization. The AC characteristics of OLEDs are of interest because the proposed driving method of OLEDs is by an AC waveform and many device characteristics such as capacitance, trapping and detrapping of charge carriers, and response times can be obtained from AC assessment. In this thesis three, novel methods for characterizing OLEDs, denoted steady-state (*i.e.* steady-state with the applied voltage waveform) transient current-transient voltage [i(t)-v(t)], steady state transient brightness-transient voltage [b(t)-v(t)], and steady-state transient brightness-transient current [b(t)-i(t)] , using AC waveform excitation are proposed and developed. These methods offer a more complete way of characterizing OLEDs and provide insight into many phenomena not observed pre-

viously in OLEDs. In addition, by employing these methods as the OLED is aged, a better understanding of the aging mechanism may be obtained.

The goal of the research presented in this thesis is to develop new methods of characterization of the current transport and optical properties of OLED-based devices. The organization of the thesis is as follows. Chapter 2 consists of a review of the device physics of OLEDs and an overview of the relevant literature. Chapter 3 presents the experimental methods used. Chapter 4 describes experimental results, including important results of each of the characterization techniques. Chapter 5 consists of preliminary aging results utilizing the novel analysis methods developed in this thesis. Finally, Chapter 6 contains conclusions and recommendations for future work.

Chapter 2
Literature Review of Organic Light-Emitting Devices

This chapter contains a literature review and a review of the device physics of OLEDs.

2.1 Device Structure

2.1.1 Small Molecule OLED

The basic device structure of the OLEDs considered in most of this thesis presumed to be very similar to the devices first proposed by Tang *et al.*, as shown in Fig. 2.1. [3] The OLED stack is deposited onto an indium-tin-oxide (ITO) coated glass substrate, with the ITO forming the anode. A hole injection layer (HIL) of CuPc is deposited directly onto the ITO. Then, a hole transport layer (HTL) of naphthyl-substituted benzidine derivative (NPB), an electron transport layer (ETL) of 8-hydroxyquinoline aluminum (Alq_3), and a Mg:Ag cathode are deposited. The OLED is driven by making electrical contact to the anode and cathode and applying a positive bias of at least 5 V. Light generation takes place in the ETL and photons pass through the device to exit through the substrate. The Alq_3 layer emits green light. When a color other than green is desired, a dye layer is inserted or mixed into the ETL. Organic dyes are available for almost any visible color desired. The small molecule OLEDs discussed in this thesis were provided by the Eastman Kodak Company. [2]

2.1.2 Polymer LEDs

In this thesis polymer light-emitting devices (PLEDs) are also investigated. Note that in this thesis the acronym PLED is used when discussing issues specific to polymer LEDs. The acronym OLED is used when addressing issues specific to small

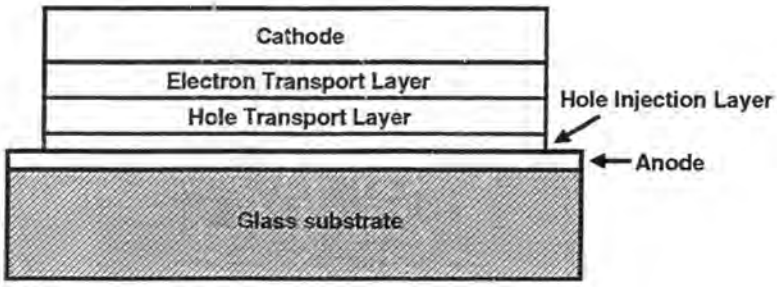

Figure 2.1. Small molecule OLED device structure.

molecule OLEDs or issues generic to both small molecule OLEDs and PLEDs. The denotation of OLED should be clear from the context of the discussion. The PLEDs studied here were provided by the UNIAX Corporation and by Professor Yang Yang of the University of California at Los Angeles (UCLA).

Little is known about the device structure of the PLEDs from UNIAX. They presumably consist of a single layer of polymer with a low work function metal contact. Typical PLEDs are constructed on glass substrates with layers deposited as follows: an anode of indium-tin oxide (ITO), a conducting polymer, a polymer layer of poly(2-methoxy,5-(2'-ethyl-hexyloxy)-1,4-phenylene vinylene) (MEH-PPV), and a cathode of Ca. The typical device structure is shown in Fig. 2.2. [4]

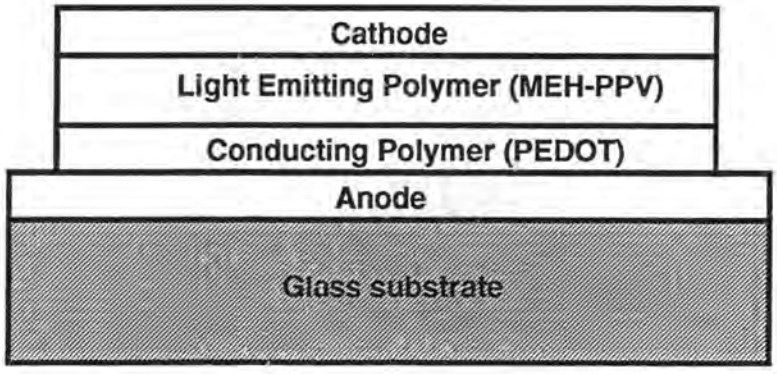

Figure 2.2. Typical PLED structure.

The devices from UCLA are deposited onto a glass substrate with an anode of ITO, a layer of 3,4-polyethylenedioxylthiophene-polystyrenesulfonate (PEDOT), followed by a layer of MEH-PPV, and a cathode of Ca and Al. The aluminum is used to protect the calcium. The layer of PEDOT is a conducting polymer than behaves similar to a metal. The MEH-PPV thickness is generally between 80 and 105 nm. Both the UNIAX and UCLA devices are encapsulated with epoxy and a glass cover to protect these devices from atmosphere. Presumably, the UCLA devices and the UNIAX devices are similar in construction.

For the PLEDs the MEH-PPV is the emission layer. Variations on the MEH-PPV polymer have been suggested for improved performance of PLEDs, as well as for changing the emission color. [5, 6] Multiple layer devices consisting of an HTL and an ETL have been proposed as well. [6] The motivation for using multiple polymer layers is to improve charge carrier balance, thereby improving efficiency.

2.2 Device Operation

The brightness of an OLED is determined by the magnitude of the current. Therefore, it is best to operate OLEDs using a constant current source in order to maintain a constant brightness. Also, it has been shown that aging characteristics of small molecule OLEDs are improved if the OLED is subjected to periodic negative biasing. [3] With this in mind, a driving waveform with a positive current source and a negative voltage source is best for improved lifetime and brightness characteristics of OLEDs.

For inorganic EL device characterization a bipolar piecewise-linear waveform is useful for electrical and electro-optic characterization. [7] In this thesis, a bipolar piecewise-linear waveform, as shown in Fig. 2.3, is employed for electro-optic characterization of OLEDs. The initial rise time (RT) is 15-150 μs, the constant maximum applied voltage pulse width (PW^+) is 0-200 μs, the intermediate transition time (ITT) is 20-300 μs. Typically, a linear transition from the positive maximum applied voltage (V^+_{max}) to the negative maximum applied voltage (V^-_{max}) is used and the fall

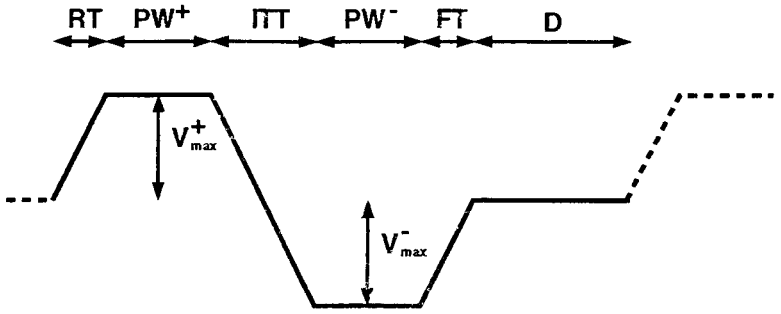

Figure 2.3. Representative applied voltage waveform for OLED testing. Waveform parameters identified are positive and negative maximum applied voltages (V^+_{max}, V^-_{max}), rise and fall times (RT, FT), and intermediate transition time (ITT).

time (FT) is 15-150 μs. Usually a ramp rate (RR) is set for use throughout the OLED waveform so that RT, ITT, and FT all have the same ramp rate. Occasionally a zero bias delay (D) portion is inserted after the negative pulse. D is usually between 0 and 1000 μs. The major difference between the applied voltage waveform used for inorganic and organic EL characterization is that the periods are much longer for the organic waveform. [7] This waveform has proven to be very useful in exploring different aspects of OLED and PLED operation. Additionally, it is similar to the bipolar waveform suggested for improved device efficiency. [3]

2.3 Device Physics

2.3.1 Small Molecule OLEDs

A few basic aspects of small molecule OLED device physics are as follows. The general characteristics of the HTL are that the electron mobility is very small compared to the hole mobility and the hole mobility of the HTL is relatively large compared to the electron mobility of the ETL. [1, 2] For a typical diamine HTL the hole mobility is 10^{-2} to 10^{-4} $cm^2V^{-1}s^{-}1$ (the hole mobility of a diamine HTL is about 1000 times the electron mobility of an Alq_3 ETL). [2] An Alq_3-based ETL is thought to possess an exponential distribution of traps. [8] The hole mobility in an Alq_3 ETL is

$2 \times 10^{-8} cm^2 V^{-1} s^{-1}$ and the electron mobility is $1.4 \times 10^{-6} cm^2 V^{-1} s^{-1}$. [9] However, note that the hole mobility is large enough that holes can still transport through the ETL. Also, the mobility of Alq_3 is strongly field- and temperature-dependent. The Alq_3 mobilities quoted previously were obtained at an electric field of 0.4 MV/cm and at room temperature. Note that Hosokawa *et al.* estimated an electron mobility for Alq_3 of $(5 \pm 2) \times 10^{-5} cm^2 V^{-1} s^{-1}$ at 1 MV/cm. [10] The recombination of holes and electrons responsible for the OLED light output occurs in the ETL near the ETL/HTL interface. [2] Electron and hole recombination and the subsequent emission of a photon is thought to occur through exciton formation and annihilation. [2]

A discussion of charge transport in OLEDs is important because it is primarily the physics of the charge transport that determines the current-voltage (I-V) characteristics of OLEDs. It is useful to distinguish between injection-limited (IL) and bulk-limited (BL) transport when considering charge transport in OLEDs. IL devices are characterized by charge transport properties that depend on the injection of charge from the electrodes into the device. Generally, when a large energy barrier exists at electrode interfaces, inhibiting the injection of carriers, devices tend to be IL. Conversely, when the energy barrier at the interface is small and the bulk carrier mobility is low, charge transport tends to be BL. With BL transport, the bulk properties of the device dominate the charge transport physics and establish the I-V characteristics.

At the present time it is generally believed that OLEDs are BL when a low work function metal is used as a cathode electrode. BL transport can be further broken down into space-charge-limited (SCL) conduction and trapped-charge-limited (TCL) conduction. SCL conduction typically occurs in insulating materials that are relatively free of traps. With SCL conduction, a carrier build up occurs within the device; the electric field associated with this space charge build up inhibits carrier transport. As more carriers are injected, the carrier concentration increases near within the device, resulting in the formation of space charge. The presence of this space charge limits the transport of carriers; thus, the conduction is space-charge-

limited. SCL conduction is characterized by

$$J = \frac{9\epsilon\mu V^2}{8d^3}, \tag{2.1}$$

where V is the voltage dropped across the insulating layer at which injection is occurring, d is the thickness of the insulating layer, ϵ is the permittivity, and μ is the mobility . Equation 2.1 is referred to as Child's law. [11, 12, 13, 14] The above equation is valid for a single carrier and single layer device. However, if the current conduction is limited by conduction through a single layer and it is dominated by conduction of one carrier type, Eq. 2.1 should be valid for the case of dual carrier, multi-layer OLEDs.

TCL conduction occurs when current conduction is limited by the capture and emission of carriers from traps. Generally, materials that are TCL have a large concentration of traps that interact with injected carriers. For OLEDs, the trap distribution in Alq_3 is thought to increase exponentially as the conduction band edge is approached. [8] In the TCL model some of the injected charge is captured in traps, reducing the free carrier concentration and hence limiting the amount of current that can flow. Current conduction in a TCL with an exponential trap distribution material is described by

$$J = q^{1-l}\mu N_c \left(\frac{2l+1}{l+1}\right)^{(l+1)} \left(\frac{l}{(l+1)}\right)^{l} \left(\frac{\epsilon}{N_t}\right)^{l} \frac{V^{(l+1)}}{d^{(2l+1)}}, \tag{2.2}$$

where μ is the mobility, N_c is the density of states in the conduction band, $l = \frac{T_c}{T}$, T_c is the characteristic temperature of the traps, T is the device temperature, ϵ is the permittivity, N_t is the trap density, V is the voltage drop across the insulating layer, and d is the insulator thickness. [11, 12, 13, 14] As with SCL conduction, Eq. 2.2 is valid for a single carrier single layer device. However, if the current conduction is limited by conduction through a single layer and it is dominated by conduction of one carrier type, Eq. 2.2 should be valid for the case of dual carrier, multi-layer OLEDs.

Throughout this thesis it is assumed that OLEDs are TCL devices. [8] For PLEDs there is still some question regarding whether they are SCL or TCL devices.

It is possible that PLEDs fabricated with different materials may give rise to either type of transport. In this thesis both TCL and SCL conduction are considered as possible conduction mechanisms for PLEDs.

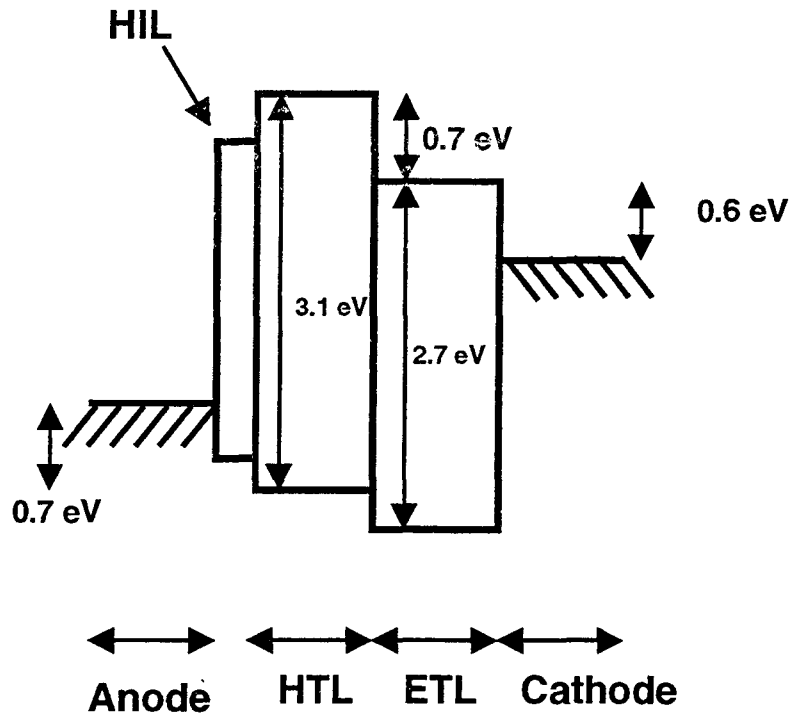

Figure 2.4. The flat band configuration of a small molecule OLED. Note that the flat band voltage is about 1.1 V. The HIL reduces the barrier presented to holes as they are injected from the anode.

Perhaps the best way to understand the operation of an OLED is through the use of energy band diagrams. However, there is some uncertainty regarding the validity of employing the energy band model for organic materials. The major difficulty with the band model arises from the narrow band widths of organic materials. [11, 12, 14] Essentially, the band width is on the order of the uncertainty in the energy of the electron. Although the validity of the band model is questionable for organic materials, it has been useful for explaining many OLED device physics properties and has proven useful in explaining many of the experimental results discussed in this thesis. [11]

As an alternative to the energy band model, molecular orbital (MO) theory is often employed in discussions of transport in organic materials. [11, 12, 14] In MO theory the lowest unoccupied molecular orbital (LUMO) and the highest occupied molecular orbital (HOMO) are used in place of the valence band maximum and the conduction band minimum, respectively. The use of LUMO and HOMO energy levels avoids issues related to the viability of employing energy band concepts in discussions of organic materials. However, LUMO and HOMO energy levels do not account for a periodic crystal structure. In this thesis, the energy band model is assumed to be valid since the conclusions that may be draw from MO theory and energy band theory are very similar.

The energy band diagrams shown in this section describe the OLED operation when it is subjected to the piecewise-linear bipolar voltage waveform described previously. The energy band diagram shown in Fig. 2.4 is typical of OLEDs studied in this thesis under flat band conditions. [15, 16] Notice that the barrier for the injection of holes into the ETL from the HTL is smaller than the barrier for the injection of electrons into the HTL from the ETL. This, and the fact the the HTL has a very low electron mobility is why the HTL is an electron-blocking layer. Also, note that the flat-band voltage is about 1.1 V.

The following energy band diagrams are ment to shown the current understanding of OLED operation. Thus, band bending due to trapping is not shown in the following energy band diagrams since it has not bee discussed in previous OLED literature. The effects of band bending due to carrier trapping are discussed in detail in Chapter 4.

Figure 2.5 shows an energy band diagram of an OLED just after the initiation of hole and electron injection from the electrodes. Holes are injected more efficiently than electrons, so that some holes are able to travel through the OLED to the cathode without recombining or being trapped. [17] Also, before the trap emission and capture rates reach steady-state, many injected electrons are trapped in the ETL. Notice that no electrons are injected from the ETL into the HTL. The HTL is known to be an effective electron blocking layer. [15]

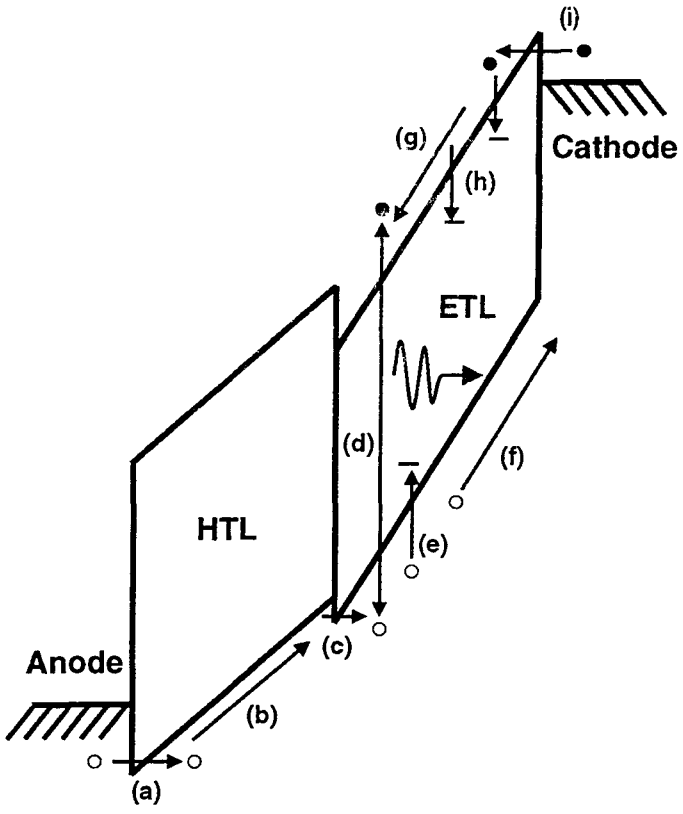

Figure 2.5. An energy band diagram of a small molecule OLED at the threshold voltage. Holes (a) are injected from the anode, (b) pass through the HTL, and are (c) injected into ETL. Near the HTL/ETL interface, (d) holes and electrons recombine, resulting in photons. (e) Some holes are trapped in the ETL, (f) while others are transported through the ETL to the cathode. (g) Electrons are transported through the ETL before recombining with holes. (h) Most injected electrons are trapped in the ETL near the cathode. (i) Electrons are injected from the cathode. Notice that the HIL has been omitted for simplicity.

Figure 2.6 shows the energy band diagram when the OLED is ramped up to a forward bias much greater than the threshold voltage (the voltage at which light is first observed). At this voltage, hole and electron injection are more evenly balanced and the trap occupancy has reached steady-state with the injected electrons so the holes are not able to pass through the ETL to the cathode before recombining. [17] Notice that if an electron is released from a trap, another quickly fills it (the capture and emission rates are balanced).

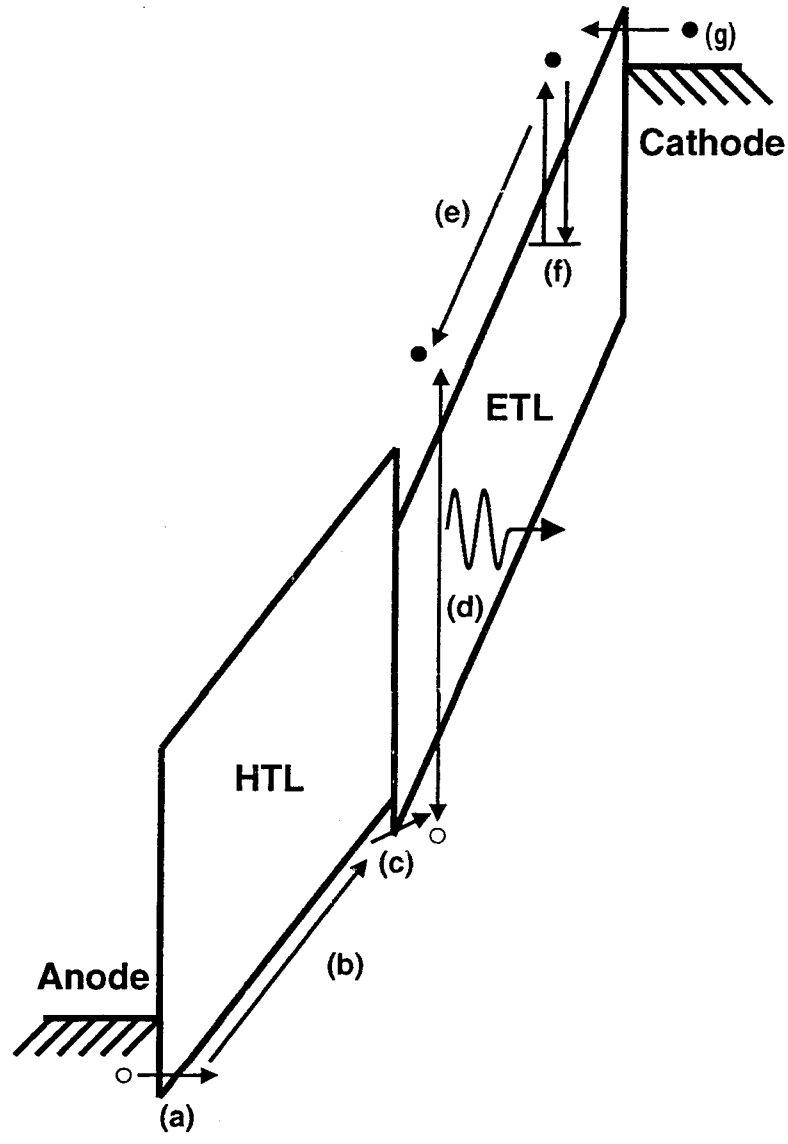

Figure 2.6. The energy band diagram of a small molecule OLED at a positive bias much greater than the threshold voltage. (a) Holes are injected from the anode, (b) transported across the HTL, and (c) injected into the ETL. (d) Holes and electrons recombine, resulting in photons. (e) Electrons are transported across the ETL. (f) The electron trap emission and capture rate is balanced. (g) Electrons are injected into the ETL from the cathode. The HIL has been omitted for simplicity.

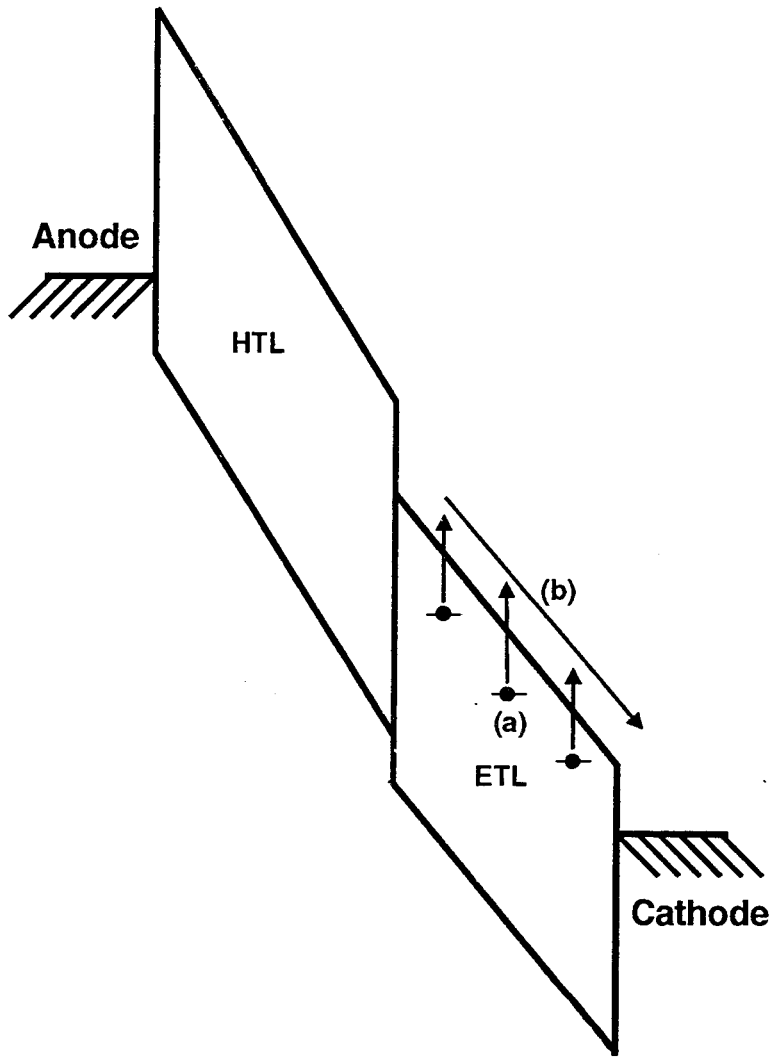

Figure 2.7. The energy band diagram of a small molecule OLED just after the applied voltage has been ramped down from a positive bias to a large negative bias. (a) Electrons in traps detrap and (b) exit the ETL. Notice that the HIL has been omitted for simplicity.

Finally, Fig. 2.7 shows the energy band diagram of an OLED when it is ramped to a negative voltage. Most of the carriers trapped in relatively shallow traps have already exited the OLED and now carriers trapped in deep traps are beginning to be released through the assistance of the applied field. The negative applied voltage appears to improve aging characteristics. [3] This improvement has been suggested to be caused by the release of trapped charge and/or the movement of ionic impurities and dipoles. [3, 18] The applied bias is then ramped up again, returning to the energy band state described in Fig. 2.4 and the cycle is repeated.

At present very little is known about the aging mechanism of OLEDs. It is known that OLED aging is very sensitive to the presence of air and water. [19] By packaging OLEDs in an inert atmosphere, aging characteristics dramatically improve. [19] Aging of OLEDs may be caused by degradation of the Mg:Ag cathode by the formation of $Mg(OH)_2$. [20] Burrows *et al.* showed that electrode nonuniformity may result in areas of extremely high field (>2 MV/cm) where an active device is more prone to decay. [19] In addition, degradation of the bulk of the organic materials comprising the OLED may cause aging. Possible causes for bulk degradation are photodegradation and reactions with water and oxygen in the bulk. [21]

2.3.2 PLEDs

The device physics of PLEDs is very similar to that of small molecule OLEDs with a few notable exceptions. Parker suggested that the conduction characteristics of MEH-PPV are governed by the tunneling of both holes and electrons though the energy barriers formed at the electrode MEH-PPV interface, suggesting that these devices are IL. [4] However, recent evidence shows that hole transport in MEH-PPV is SCL and electron transport is TCL with an exponential trap distribution having a characteristic energy of 0.1 eV. [22] Conwell and Wu conclude that the Ca cathode forms an ohmic contact with MEH-PPV. [23]

2.4 Literature Review

Tang *et al.* first introduced a practical OLED in 1987. [1] This OLED is constructed on a glass substrate and consists of a thin-film stack comprised of a transparent ITO anode, an aromatic diamine HTL, an Alq_3 ETL, and a Mg:Ag cathode. Tang *et al.* then demonstrated that an OLED could be made to emit in many different colors through the use of different dopant molecules in the ETL. [2] The basic OLED was improved by the addition of a CuPc HIL between the anode and the HTL, by replacing the daimine HTL with a naphthyl-substituted benzidine derivative (NPB) HTL, and by driving the OLEDs with a bipolar voltage waveform. [3]

Burrows *et al.* suggested that OLEDs based on Alq_3 may be trapped-charge-limited (TCL). [8] They showed that a current-voltage (I-V) curve of Alq_3 OLEDs follows a power dependence on applied voltage, indicating TCL conduction. In addition, they showed that the the TCL current was consistent with an exponential trap distribution in the Alq_3 with a characteristic energy of about 0.1 eV ($k_bT_c = 0.1$ eV). However, counter to the TCL model, Matsumura *et al.* proposed that the I-V characteristic are limited by charge injection into the HIL and ETL. [24] Matsumura *et al.* were able to fit I-V data to their IL model at least as well as the TCL model, although the dielectric constant they used did not reflect the experimental dielectric constant of the organic ETL. Their argument for adjustment of this dielectric constant is that the metal/organic interface forms a barrier layer for injection of carriers, modifying the dielectric constant. Evidence for TCL conduction is presented in this thesis.

Yang and Shen have had some success modeling small molecule OLEDs using the TCL model. [25, 26] They show that a distribution of hole and electron traps, as well as the presence of dye layers, can effect where the recombination zone is located in the ETL. Their model is useful in explaining why some OLEDs with dye layers show emission from both the Alq_3 and from the dye molecule while other OLEDs only show emission from the dye layer.

Matsumura *et al.* relate the width of the emission zone to the applied voltage. [17] They assert that the emission zone at low applied voltage is wider than it is at high applied voltage. At low voltage, the injection of electrons is difficult and holes are able to drift further into the ETL before recombining with electrons. At high voltages, most of the voltage drop in the OLED is across the ETL, due to a lower ETL mobility than HTL mobility, and electron injection is improved.

The ability to model OLEDs via a computer simulation program such as SPICE is an important step in constructing a practical OLED display. Bender *et al.* have shown that an accurate SPICE model can be obtained for the DC mode of operation. [27] However, when this model is compared to data taken using an AC waveform, it fails to accurately account the hysteretic nature of the i(t)-v(t) curves of actual OLEDs.

It has been shown that lower OLED threshold voltages may be obtained via the addition of a very thin LiF layer between the cathode and the ETL. [28, 29, 30] The LiF is believed to modify the interfacial barrier of the cathode, thus improving electron injection. In addition, Al/LiF cathodes were shown to have better I-V characteristics than Mg/LiF or Mg cathodes. Similar results are found when a Al_2O_3 layer is inserted between an Al cathode and the ETL. [31]

The use of a bipolar applied voltage waveform has been shown by VanSlyke *et al.* to improve the aging characteristics by allowing time for the OLED to be exposed to a negative bias voltage. [3] Zou *et al.* performed qualitative experiments documenting the effects of this kind of negative bias treatment and suggested that the improvement in threshold voltage is due to electric dipole alignment and movement of ionic impurities. [18]

Egusa *et al.* used an extremely low frequency ($\leq$ 1 Hz) triangle waveform to generate i(t)-v(t) and b(t)-v(t) curves for OLEDs. [32, 33] The method of Egusa *et al.* is similar in some respects to the analysis methods developed in this thesis. However, the waveforms used in this thesis are much higher frequency (1-5 kHz) and are not triangle waveforms.

The results presented in this thesis are interpreted in terms of a model similar to the model for OLED operation introduced by Khramtchenkov *et al.* in which hole accumulation at the ETL/HTL interface plays an important role in OLED operation. [34, 35] However, Khramtchenkov *et al.* consider the DC mode of OLED operation only and do not consider the possibility of charge trapping in the OLED.

Chapter 3
Experimental Techniques

In this chapter the experimental techniques developed for OLED characterization are described.

3.1 Setup

The experimental setup, as shown in Fig. 3.1, consists of an arbitrary waveform generator (AWG), a personal computer, a digital oscilloscope, a sense resistor, the OLED under test, and a photomultiplier tube (PMT). With this setup, voltage waveforms are generated with the AWG, amplified by the amplifier, and applied to the device under test. The voltages $v_1(t)$, $v_3(t)$, and $v_4(t)$ represent probe voltages measured by the oscilloscope. The probe voltage $v_2(t)$, not shown in Fig. 3.1, is used for synchronization between the AWG and the oscilloscope. From the probe voltages, the voltage [v(t)] applied to the OLED, the current [i(t)] through the OLED, and the brightness [b(t)] are calculated and displayed by the computer. The applied voltage is defined as

$$v(t) = v_1(t) - v_3(t) \tag{3.1}$$

and the current through the device is defined as

$$i(t) = v_3(t)/R_{sense}. \tag{3.2}$$

The probe voltage $v_4(t)$ is a sense voltage from the PMT which is proportional to b(t).

The amplifier circuit is specifically designed for OLED testing and aging studies. The amplifier has two modes: a test mode and an aging mode. In the test mode, the amplifier acts as a simple voltage amplifier with a gain of approximately 3. In the aging mode, the amplifier outputs a current when a positive voltage is input and an amplified negative voltage when a negative voltage is input. The mode is selected via

computer control. Thus, periodic characterization of the OLED can be performed automatically during aging.

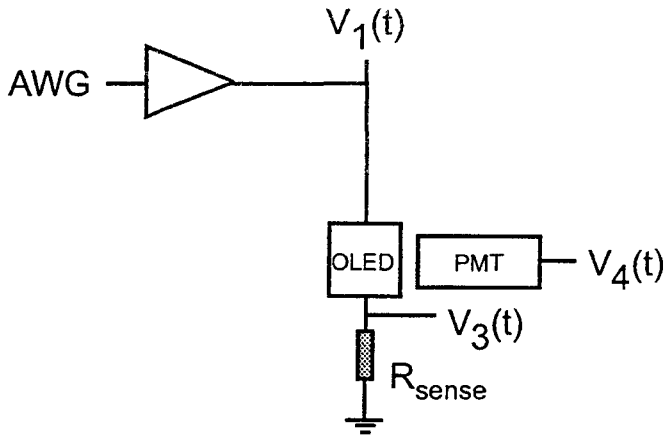

Figure 3.1. The circuit used for OLED testing and aging studies. The voltages $v_1(t)$, $v_3(t)$, and $v_4(t)$ are monitored by the oscilloscope and $v_2(t)$ (not shown) goes from the arbitrary waveform generator (AWG) to the oscilloscope for synchronization. The sense element is a resistor, typically 19.1 Ω.

The resistance of the sense resistor must be chosen carefully. The larger the sense resistor, the more voltage dropped across it; this results in greater measurement sensitivity. However, a larger sense resistor results in a larger RC constant of the measurement circuit, so that the applied voltage is distorted from the actual waveform programmed into the AWG. The amount of voltage distortion of the applied voltage waveform is equal to the IR drop across the sense resistor, and is thus proportional to the current flowing through the OLED; since the current flowing through an OLED is nonlinear with respect to voltage, the applied waveform voltage distortion is also nonlinear. It is best to use a small sense resistor (*e.g.* 19 Ohms) when little distortion in v(t) is desired (*e.g.* for i(t)-v(t), b(t)-v(t), and i(t)-b(t) analysis). A large sense resistor (500 Ohms) should be used for DC experiments or when transient information is not required and accuracy in determining i(t) is required (*e.g.* I-V, $Q_{detrapped}$-$Q_{transferred}$, and $Q_{detrapped}$-PW^+ analysis).

3.2 DC Experiments

For DC experiments the applied voltage is stepped from one DC level to the next. At each DC level the system is allowed to reach steady-state and then it is averaged. The DC applied voltage (V) and current (I) are obtained from the DC equations equivalent to Eq. 3.1 and Eq. 3.2, respectively.

3.2.1 Current-Voltage (I-V) Analysis

A typical current-voltage (I-V) plot is shown in Fig. 3.2. DC I-V plots have been shown to be useful in establishing the current transport physics of OLED devices. [8] Generally, if a measured I-V plot may be fit to Eq. 2.2 then the OLED operates under TCL conditions and the trap distribution can be determined by assessment of parameter "l" in Eq. 2.2. Typically, OLEDs devices operate under TCL conditions. [8] If the OLED operates under IL or SCL conditions then this should be reflected in the measured I-V curves.

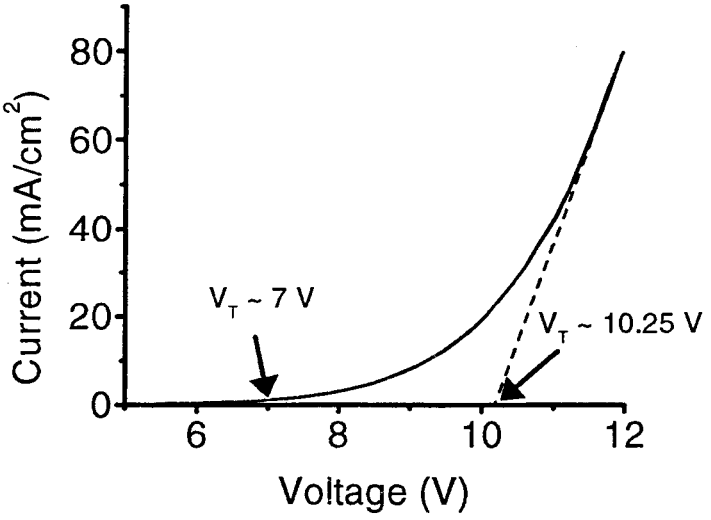

Figure 3.2. A representative I-V curve of an OLED. The threshold voltage, V_t, is estimated to be 10.25 V by linear extrapolation of the I-V curve back to the voltage axis. The threshold voltage, V_t, is estimated to be 7 V for a current of 1 mA/cm^2.

The threshold voltage, V_t, is an important parameter characterizing the operation of OLEDs. In general it is the voltage at which the OLED begins to function in a useful manner (*i.e.* emits light). However, this definition must be very carefully specified so that the V_t for a given OLED is the same regardless of the equipment being used for measurement. Also, V_t should reflect the device physics of the OLED and should not depend on OLED parasitics. The voltage at which brightness is detected is a poor definition for threshold voltage since it depends on the detection threshold of the light measuring equipment.

A better definition for V_t is the voltage at which the brightness reaches a minimum threshold level (*e.g.* 0.1 cd/m^2). This definition for V_t requires that the optical detector used in measurement be precisely calibrated. In this thesis data was taken using an uncalibrated PMT. Thus, this minimum threshold level definition is not practical for this thesis.

An alternative would be to define V_t as the voltage at which the current reaches a given value (*e.g.* 1 mA/cm^2), as shown in Fig. 3.2. This definition assumes that the current and brightness are proportional by a fixed value. This is a good assumption, as discussed in Sec. 3.2.2. However, the proportionality between current and brightness may change as the OLED is aged. A change in proportionality implies that the current threshold does not correspond to the same brightness for all OLEDs. This definition for V_t is used in this thesis for the sake of simplicity.

Another possibility for defining V_t would be to linearly extrapolate a I-V or B-V curve back to its intercept on the voltage axis, as shown in Fig. 3.2. Unfortunately, the linear portion of a I-V and B-V curve is related to the series resistance of the OLED. Thus, the resulting V_t does not reflect the device physics of light generation, but is more of a characteristic of the series resistance.

The final method for finding V_t is to linearize the I-V or B-V curve by applying an appropriate mathematical transform to the current or brightness versus voltage curve. Typically, the brightness and current are related to voltage by a power law dependence via Eq. 2.2. Notice that the power law dependence is based on the term l. Therefore, a linearization of current or brightness is accomplished by taking the

l^{th} root of current or brightness and plotting it against voltage. These transformed I-V or B-V curves are then linearly extrapolated back to the voltage axis and V_t is defined as the intercept with the voltage axis. This method results in a well defined V_t that reflects the relevant device physics and is not dependent on the equipment. The problem with this method is that it is complex and the value of l must be known to a high degree of accuracy. The l term differs from device to device and it must be determined from a power law fit to the I-V or B-V curve. Thus, this transformation procedure for assessing V_t can be difficult and may contain some ambiguity if the value of l is not well defined.

V_t should be determined exclusively from DC measurements since the AC measurements described herein have hysteresis and displacement current, which make accurate determination of V_t difficult. Also, the AC measured characteristics are dependent on the waveform parameters. Thus, different waveform parameters would result in different V_t's.

3.2.2 Brightness-Current (B-I) and Brightness-Voltage (B-V) Analysis

For most OLED materials brightness is proportional to current transported through it. Thus, B-I curves for OLEDs are linear. [2] The proportionality constant between B and I is defined as

$$\alpha = B/I. \tag{3.3}$$

The constant α is useful in understanding AC b(t)-i(t) analysis, as discussed in Section 3.3. Since a B-V curve (not shown) is simply proportional to the I-V curve by α, the B-V curve is not shown in subsequent OLED characterization. α is directly related to the quantum efficiency of the OLED since it relates current (electrical flux) to brightness (photon flux). The quantum efficiency is the number of charge carriers that produce photons and it is usually expressed as a percentage.

3.3 AC Experiments

For the AC experiments performed in this thesis, a bipolar, piecewise-linear applied voltage waveform is employed, as shown in Fig. 2.3. Typical waveform parameters are positive and negative maximum applied voltage amplitudes (V^{+}_{max}, V^{-}_{max}) of 5-15 V, ramp rate (RR) of 0.1 V/μs, positive and negative pulse widths (PW^{+}, PW^{-}) of 50-500 μs, a delay time (D) of 0-1000 μs, and repetition frequency of 1 kHz to 5 kHz. Note that positive and negative refer to applied voltage polarities in which the OLED is forward- and reverse-biased, respectively. Typically, the applied voltage waveforms consist of a positive voltage pulse at the beginning of the voltage waveform and a negative voltage at the end of the voltage waveform; a zero voltage delay portion, D, is sometimes inserted after the negative pulse. However, an inverted applied voltage waveform is also sometimes employed in which the initial voltage is negative and the trailing voltage is positive in the applied voltage waveform. In this thesis, a standard waveform is defined as: $V^{+}_{max} = -V^{-}_{max} = 12V$, RR = 0.1 V/$\mu$s, $PW^{+} = PW^{-} =$ 200 μs, and D = 0 μs. Unless otherwise noted, the standard waveform parameters are used throughout this thesis.

v(t), i(t), and b(t) data is obtained only after the OLED has reached a steady-state with the applied voltage waveform. Thus, the AC measurements are referred to as steady-state transient measurements, which seems contradictory until it is recognized that steady-state is with respect to the applied voltage waveform. The OLED is in steady-state with the applied voltage waveform and the transient v(t), i(t), and b(t) characteristics are measured.

3.3.1 OLED Current Components

For certain measurements developed in this thesis it is useful to employ the equivalent circuits shown in Fig. 3.3 in order to clarify the nature of the current which flows in an OLED. [36] Circuit A is obtained by mapping the ETL and HTL into an equivalent parallel network consisting of capacitor and a nonlinear, voltage-controlled current-source. Circuit B is a simplified equivalent circuit derived from A. C_{ETL}, C_{HTL}, and

C_t are the ETL, the HTL, and the total OLED stack capacitance, respectively. The voltages v_{ETL}, v_{HTL}, and v are the voltage drop across the ETL, the HTL, and the entire OLED, respectively. The currents i_{ETL}, i_{HTL}, and i_c are the ETL, HTL, and total conduction current, respectively. Note the total current is given by

$$i(v) = C_{ETL}\frac{dv_{ETL}}{dt} + i_{ETL}(v_{ETL}) = C_{HTL}\frac{dv_{HTL}}{dt} + i_{HTL}(v_{HTL}) = C_t\frac{dv}{dt} + i_c(v). \quad (3.4)$$

From the fact that Circuit A and B are equivalent, it can be shown that

$$i_c(v) = \frac{C_{ETL}}{C_{HTL} + C_{ETL}} i_{HTL}(v_{HTL}) + \frac{C_{HTL}}{C_{HTL} + C_{ETL}} i_{ETL}(v_{ETL}). \quad (3.5)$$

Thus, if $i_c(v)$ is obtained via a simple baseline subtraction of the displacement current from an i(t)-v(t) curve, as discussed in Section 3.3.2, it should be recognized that the resulting conduction current involves a weighted average of the current flow across both the HTL and ETL, as specified by Eq. 3.5. Moreover, Eq. 3.5 is valid only if it is assumed that no trapping occurs in the ETL or HTL, since Eq. 3.5 is established from Circuit A in which charge can only be stored at the ETL/HTL interface.

If trapping occurs within the ETL or HTL, Circuit A is not appropriate since some of the transported charge travels only part way across the phosphor when trapping or trap remission occurs. For such a situation it is convenient to model the current as comprised of three components due to displacement, conduction and trapping. Since most researchers assert that trapping and recombination occurs predominately in the ETL, the remaining discussion will focus exclusively on the ETL. In this context, ETL conduction current, i^c_{ETL}, is meant to denote the transport of electrons and holes which result in electron-hole annihilation within the ETL. Additionally, trapping current, i^t_{ETL}, refers to the transport of electrons or holes which do not result in electron-hole annihilation within the ETL. This definition of trapping current includes the possibility of electron or hole transport across the entire length of the ETL without electron-hole annihilation, as well as the transit of an electron part way across the ETL, where it is trapped or from which it is re-emitted from a trap.

Note that this conduction/trapping current discussion is admittedly vague and appears confusing. The motivation for defining conduction and trapping current

in this manner is to account for current due to transported carriers which do not contribute to the OLED brightness. However, it is difficult to clearly articulate and quantify these ideals in the context of two-terminal OLED characterization and simplified equivalent circuits such as shown in Fig. 3.3. A more lucid treatment of carrier transport, trapping, trap re-emission, and annihilation requires employing more complicated device models in which the continuity equation is explicitly considered.

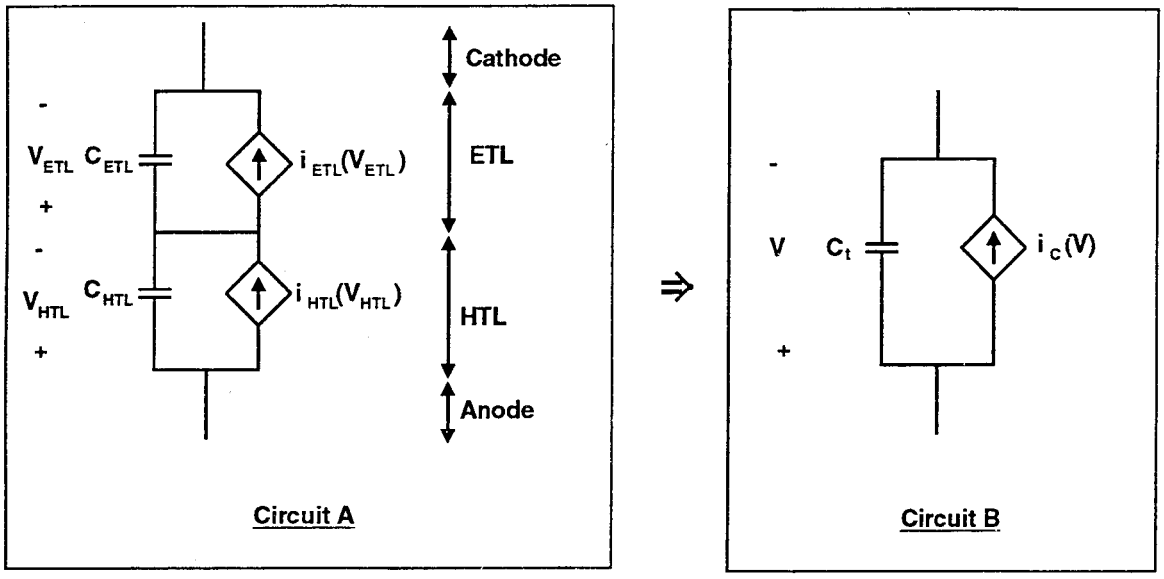

Figure 3.3. Two equivalent circuits for OLEDs.

3.3.2 Steady-State Transient Current-Transient Voltage [i(t)-v(t)] Analysis

Steady-state transient current-transient voltage [i(t)-v(t)] analysis is probably the most useful OLED characterization technique developed in this thesis. It consists of plotting the instantaneous current [i(t)] against the instantaneous applied voltage [v(t)] as the bipolar waveform described above is applied to the OLED. Additionally, i(t)-v(t) measurements are accomplished after the OLED has reached steady-state with the applied voltage waveform. A representative i(t)-v(t) curve is shown in

Fig. 3.4. Positive and negative voltages correspond to forward- and reverse-bias, respectively. The measured current corresponds to a superposition of the conduction current [$i_c(t)$] flowing through the OLED, and the displacement current arising from the C_t dV/dt current associated with the capacitive nature of the OLED. Below the threshold voltage there is a negligible amount of conduction current so that the measured current is exclusively displacement current. Thus, for these below-threshold, horizontal, baseline portions of the i(t)-v(t) curve, the physical capacitance of the entire OLED stack, C_t, may be estimated as the current divided by the ramp rate (RR),

$$C_t = \frac{i(t)}{\frac{\partial v(t)}{\partial t}} = \frac{i(t)}{RR}. \tag{3.6}$$

Notice that the capacitance data can be derived from i(t) and v(t) data by an equation similar to Eq. 3.6 but with capacitance evaluated at each v(t) and i(t) for the ramping portions of the applied voltage waveform. As long as the RR is constant for all of the ramping portions of the applied voltage waveform, the instantaneous capacitance, c(t), will be proportional to i(t) by 1/RR. C(t)-v(t) curves are typically not pltted since they are proportional to i(t)-v(t) curves.

It is sometimes found that the subthreshold portion of the i(t)-v(t) curves are not horizontal, but have a small amount of positive slope. This is attributed to a parasitic parallel resistance, R_p. R_p is equivalent to a resistor in parallel with C_t. This resistance is believed to be caused by the leakage of charge across the entire OLED stack. The parasitic parallel resistance evaluated below V_t is given by

$$R_p = \frac{\partial v(t)}{\partial i(t)}, \tag{3.7}$$

for $v(t) < V_t$. Typically, R_p is too large to be measured for OLEDs. However, for certain PLEDs R_p is small enough to result in a noticeable skewing of the measured i(t)-v(t) characteristics. For PLEDs it is believed that a significant amount of injected holes may transport completely through the polymer layer without recombining with injected electrons. This hole current may be responsible for the small R_p observed with PLEDs.

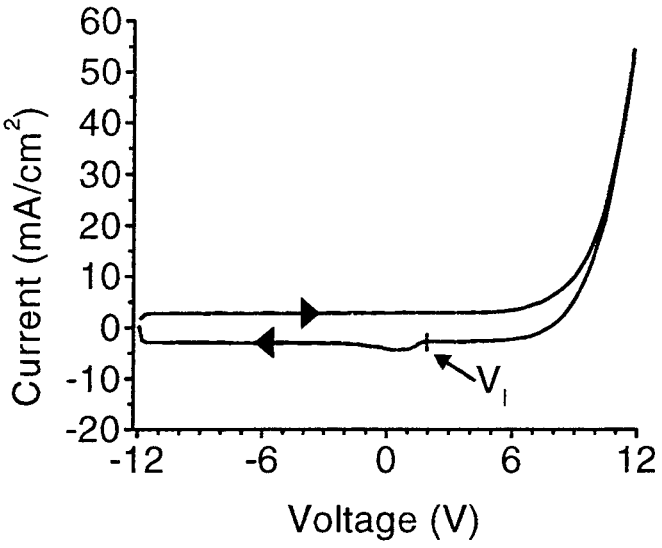

Figure 3.4. A representative i(t)-v(t) curve for an OLED. Positive and negative voltage corresponds to forward- and reverse bias, respectively. Negative and positive going portions of the waveform are indicated by respective arrows. The detrapping bump is found near the zero voltage portion of the negative going trace. The current bump initiation voltage, V_I, is indicated by an arrow.

For most of the OLEDs tested in this thesis, the current at large applied forward voltages appears to be linear with voltage, implying the existence of a limiting bulk resistance. This resistance is denoted the series resistance, R_s, because it may be modeled as a resistor in series with C_t and i_c. The current is series resistance limited by R_s if the measured i(t)-v(t) curve becomes linear at large forward applied voltages. The maximum possible value of R_s may be estimated from the slope of the linear portion of the forward biased i(t)-v(t) curve,

$$R_s = \frac{\partial v(t)}{\partial i(t)}. \tag{3.8}$$

R_s is usually only large enough to be measured for PLEDs.

A major feature of some i(t)-v(t) curves is the bump found at the bottom center portion of the i(t)-v(t) curve. This bump occurs as the applied voltage waveform transitions from a forward bias to a reverse bias. This current bump was initially attributed to detrapping of charge in the OLED phosphor layer (most likely, the

ETL). However, the current bump is more likely due to the release of holes that have accumulated at the ETL/HTL interface and charge detrapping, as discussed in Chapter 4. An important parameter related to the current bump is the voltage at which it initiates, V_I, as indicated in Fig. 3.4.

3.3.3 Steady-State Transient Brightness-Transient Current [b(t)-i(t)] Analysis

Brightness is approximately proportional to the electron/hole recombination current transported through the ETL [$i^c_{ETL}(t)$] by the proportionallity constant, α, as in the DC case. In the DC case i^c_{ETL} is equal to the total current through the OLED. Current contributions due to trapping, $i^t_{ETL}(t)$, are most likely small for OLEDs but may be significant for the PLEDs. A typical b(t)-i(t)/B-I plot is shown in Fig. 3.5 where B-I is the DC brightness-current characteristic. Notice that the portion of curve corresponding to the ramp up in applied voltage is offset along the current axis from the portion of the curve corresponding to the ramp down in applied voltage. When the current offset of the positive [or negative] ramping portion of the b(t)-i(t)/B-I curve is considered, the current offset is denoted $i^+_{offset}(t)$ [$i^-_{offset}(t)$]. Assuming that b(t) depends only on the current component $i^c_{ETL}(t)$, this AC curve offset is exclusively due to the nonradiative current components $C_{ETL}\frac{dv_{ETL}}{dt}$ and $i^t_{ETL}(t)$.

3.3.4 Steady-State Transient Brightness-Transient Voltage [b(t)-v(t)] Analysis

A representative b(t)-v(t) curve is shown in Fig. 3.6. Assuming that b(t) is proportional to $i^c_{ETL}(t)$, a b(t)-v(t) curve should result in a curve that is proportional to an $i^c_{ETL}(t)$-v(t) curve. However, note that it is much easier to obtain an experimental b(t)-v(t) curve than an $i^c_{ETL}(t)$-v(t) curve because the measured current, i(t), equal to $C_{ETL}\frac{dv_{ETL}}{dt} + i^c_{ETL}(t) + i^t_{ETL}(t)$. Thus, a b(t)-v(t) curve is useful for assessing the hysteretic nature of the ETL conduction current, and as discussed more completely in Chapter 4.

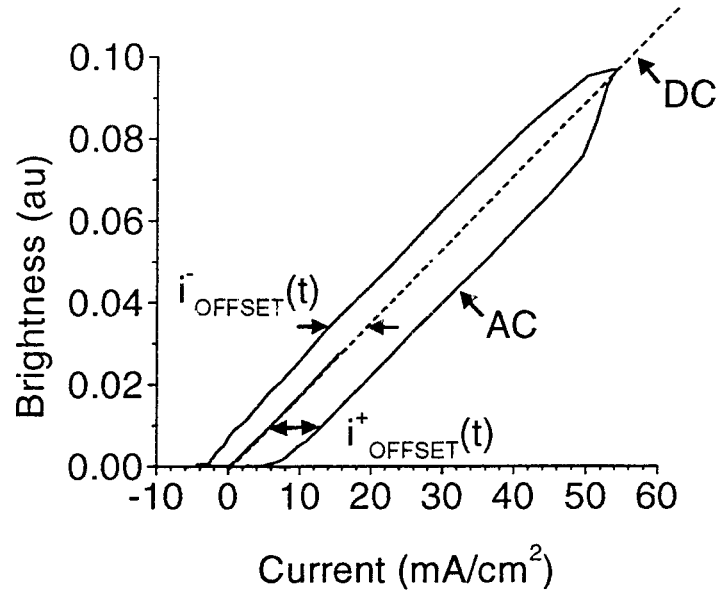

Figure 3.5. Typical b(t)-i(t)/B-I curves indicated by AC and DC, respectively. The brightness is roughly linear with current during the rising and falling portions of the applied voltage waveform. Negative and positive going portions of the waveform are indicated by respective arrows. Notice that the B-I and b(t)-i(t) curves have approximately the same slope.

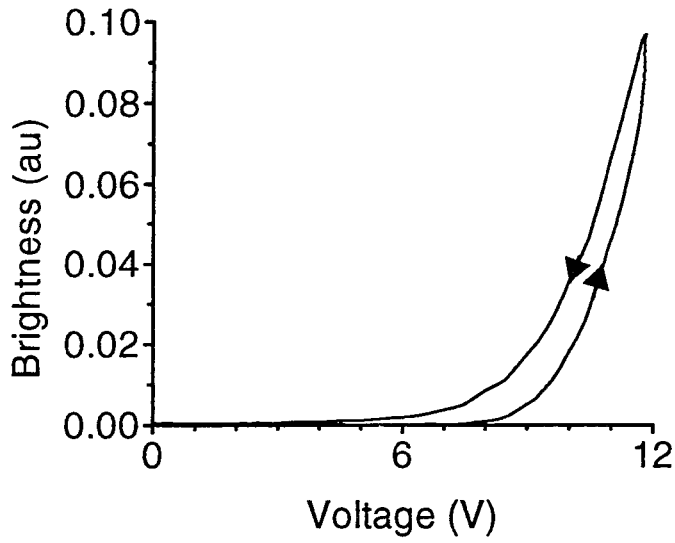

Figure 3.6. A representative b(t)-v(t) curve for an OLED. The curve has counter-clockwise hysteresis, as indicated by the respective arrows.

3.3.5 Steady-State Transient Current [i(t)] and Transient Brightness [b(t)] Analysis

Viewing transient current [i(t)], brightness [b(t)], or voltage [v(t)], responses subject to a given applied voltage waveform often provides insight into the nature of OLED device physics performance. Notice that the data used to plot the transient curves is also used to generate the i(t)-v(t), b(t)-v(t), and b(t)-i(t) curves. Representative v(t), b(t), and i(t) curves are shown in Fig. 3.7. The analysis of transient curves reveals features of OLED behavior that cannot be seen in other plots. For example, a brightness bump often occurs after a current bump; by viewing b(t) and i(t) curves concomitantly, the temporal relationship between brightness and current events becomes apparent.

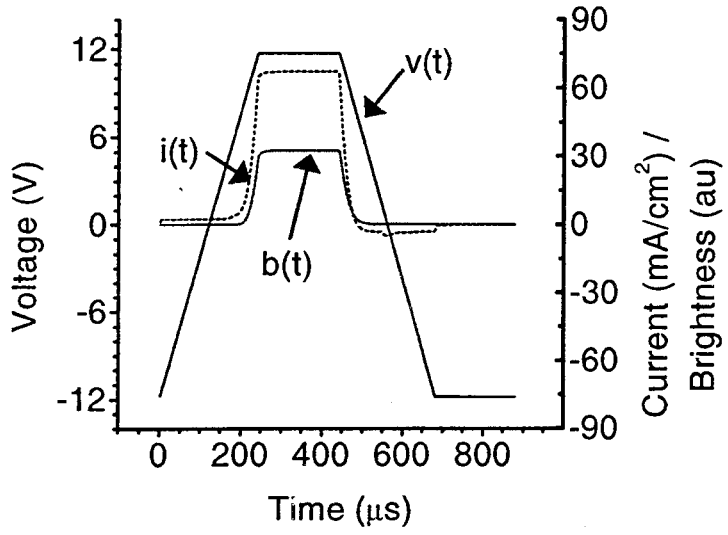

Figure 3.7. Representative v(t), i(t), and b(t) transient curves for an OLED. Brightness is in arbitrary units and on the same scale as current.

3.3.6 Detrapped Charge Analysis

In order to better understand how the charge is trapped, detrapped, accumulated, and released in OLEDs, methods for calculating the total charge detrapped/released

($Q_{detrapped}$) and the total charge transferred ($Q_{transferred}$) are developed in this thesis. $Q_{detrapped}$ is a generic term referring to electrons that detrap in the ETL and exit through the cathode and holes that are released from the ETL/HTL interface that exit through the anode. The total charge detrapped/released is found by integrating i(t) from the time corresponding to when the applied voltage is approximately equal to the V_t on the downward ramping portion of the waveform, t_1, to the time when the applied voltage is approximately equal to the V_t on the upward ramping portion of the waveform, t_2. Notice that an accurate determination of the V_t is not critical for $Q_{detrapped}$ assessment. Thus, total detrapped/released charge is found as follows,

$$Q_{detrapped} = \int_{t_1}^{t_2} i(t)dt. \tag{3.9}$$

Notice that in Eq. 3.9 the displacement charge due to the entire OLED stack cancels out of the integral; thus, effectively only the bump portion of current is integrated. The total charge transferred is calculated in a similar way

$$Q_{transferred} = \int_{t_2}^{t_1} i(t)dt. \tag{3.10}$$

$Q_{transferred}$ is the sum of the charge transferred due to $i_c(t)$, during the forward bias portion of the applied voltage waveform.

$Q_{detrapped}$ and $Q_{transferred}$ data is obtained by performing a sequence of i(t)-v(t) experiments using various PW^+ and V^+_{max} waveform parameters. For each i(t)-v(t) experiment, $Q_{detrapped}$ and $Q_{transferred}$ are calculated via Eqs. 3.9 and 3.10. A $Q_{detrapped}$-PW^+ curve is obtained by plotting $Q_{detrapped}$ versus PW^+ for various V^+_{max}'s, as shown in Fig. 3.8. This type of plot shows how the area of the current bump (current bump area is directly proportional to $Q_{detrapped}$) is affected by changes in the PW^+ applied voltage waveform parameter. The most useful type of plot obtained from this data is a $Q_{detrapped}$-$Q_{transferred}$ curve. Typically, $Q_{detrapped}$-$Q_{transferred}$ curves are plotted for a given value of V^+_{max}, as shown is Fig. 3.9. A $Q_{detrapped}$-$Q_{transferred}$ plot allows for assessment of how charge transferred during the forward bias portion of the waveform is related to detrapped/released charge. Notice from Fig. 3.9 that for small values of $Q_{transferred}$ (*i.e.* $Q_{transferred} < 10$ nC),

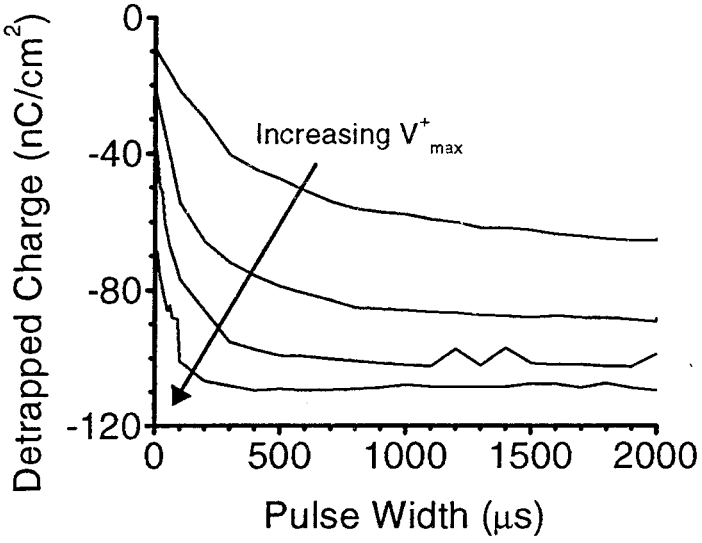

Figure 3.8. A representative set of $Q_{detrapped}$-PW$^+$ curves with V^+_{max}= 6, 7, 8, and 9 V. The arrow indicates increasing V^+_{max}. Note that decreasing $Q_{detrapped}$ indicates that more trapped and accumulated charge is released. The $Q_{detrapped}$ saturation magnitude increases with increasing V^+_{max}.

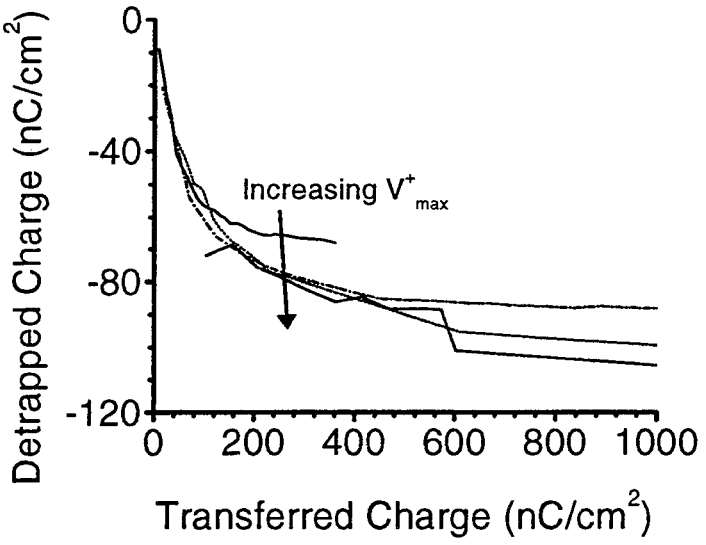

Figure 3.9. A representative set of $Q_{detrapped}$-$Q_{transferred}$ curves with V^+_{max}= 6, 7, 8, and 9 V. In the initial presaturation portion of the curve, the magnitude of $Q_{detrapped}$ is approximately equal to the magnitude of $Q_{transferred}$.

$Q_{transferred}$ is roughly equal to $Q_{detrapped}$, indicating that initially injected charge is efficiently trapped and accumulated.

3.3.7 Aging

Aging experiments are generally performed in a manner that closely approximates how an OLED would be driven in an actual display. Often OLEDs are operated in a constant-current mode. A constant-current drive results in a constant brightness because current and brightness are proportional. When the OLED is off, a negative voltage is sometimes applied in order to improve the aging characteristics of the OLED. The aging waveform used in this thesis is a square wave with the a constant-current on portion of the waveform and a negative constant-voltage off portion of the waveform. Typically, the waveform is positive 50 % of the time and negative 50 % of the time with a frequency of 60 Hz. However, other duty cycles are investigated in this thesis as well. The amount of irreversible aging is assumed to be roughly proportional to the current density. Thus, in order to standardize aging experiments, an average current density over the period of the aging waveform is set to 20 mA/cm^2 for most aging experiments. This allows for comparison between aging performed using various aging waveforms and various kinds of OLEDs.

Typically, an OLED is aged for about 120 hours (5 days) and DC and AC measurements are performed periodically throughout the aging duration. Typically, the standard AC waveform is used for AC measurements and the DC measurements are taken by stepping the applied voltage from 0 to 12 V with a 0.2 V step. When measurements are taken, the aging waveform must be interrupted and the test waveforms or DC voltages applied. The computer program stores the data obtained from these measurements immediately after the measurements are performed. This may mean that the OLED is not subjected to the aging waveform for periods as long as 30 minutes while the measurements are performed and saved. The OLED may have an opportunity to recover during the measurement period. Thus, the aging results

presented in this thesis may differ from aging results obtained using a continuously applied aging waveform. OLED recovery is discussed in Chapter 5.

Table 3.1. A summary of the experimental techniques explored in this thesis. Note that an (*) indicates a novel OLED measurement introduced in this thesis.

DC Measurements	Steady-State Measurements	Detrapped Charge Analysis
I-V B-I B-V	* i(t)-v(t) * b(t)-i(t) * b(t)-v(t) * v(t), i(t), and b(t)	* $Q_{detrapped} - PW^{+}$ * $Q_{detrapped} - Q_{transferred}$
Applied voltage (V), current (I), and brightness (B) are measured at DC levels of applied voltage.	* Two time-varying quantities are plotted parametrically after steady-state has been established between the OLED and the applied voltage waveform. However, v(t), i(t), and b(t) are not parametric plots.	* Transferred and detrapped charge ($Q_{transferred}$ and $Q_{detrapped}$) data is generated by integrating different portions of the i(t) transient curve. The resulting charges are then plotted against waveform parameters and each other.

3.3.8 Chapter Summary

Table 3.1 summarizes the OLED experimental techniques discussed in the chapter in terms of DC, steady-state, and detrapped charge measurement. Note that all of these measurements constitute novel OLED characterization methods except for the DC measurements.

Chapter 4
Experimental Results

4.1 Introduction

Throughout this chapter it should be kept in mind that little is known about the device structure of the OLEDs obtained from Kodak other than a general knowledge of the layer composition. Thus, many of the experimental interpretations provided herein are qualitative. Also, care must be taken when comparing results obtained from OLEDs of different substrates, since these devices are virtually always prepared differently. An effort is made to only make comparisons between devices from the same substrate. The results of each experiment are discussed and interpreted, first in terms of the physical device parameters that may be obtained; then in terms of the implications to the physical model used to interpret OLED operation.

4.2 DC Experiments

Although DC experiments indicating bulk-limited conduction have been reported by other research groups, it is important to note that the results presented in this thesis support the bulk-limited conduction model, as shown in Fig. 4.1. [8] Figure 4.1 shows that a power-law fits the DC I-V curves better than an exponential, indicating bulk-limited conduction, consistent with results reported Burrows *et al.* [8] It is likely that conduction current is limited by electron transport across the ETL since the Alq_3 that makes up the ETL has a very low electron mobility and is thought to possess a large trap concentration. [8, 9]

4.3 AC Experiments

AC experiments have proven to be most useful for understanding the device physics and for the extraction of OLED device parameters. The AC experimental analysis

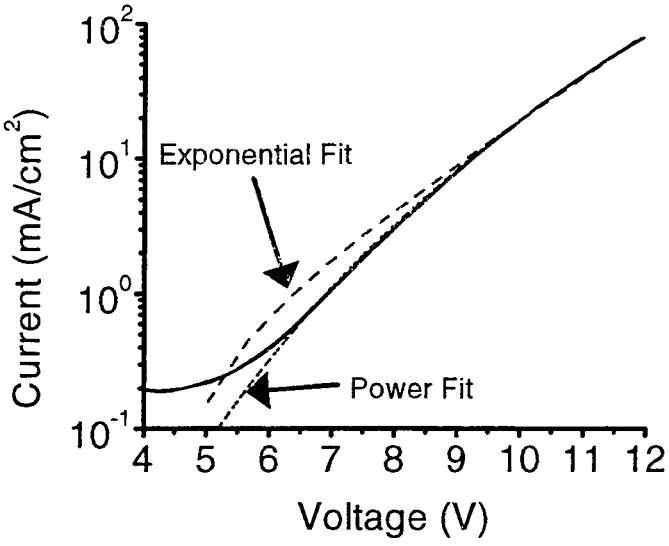

Figure 4.1. A DC I-V curve along with an exponential curve fit and a power law curve fit. Notice that the power law curve fits the experimental data much better than the exponential fit.

presented in this thesis is novel and results in new insight into the nature of OLED operation.

4.3.1 Steady-State Transient Current-Transient Voltage Analysis

From an i(t)-v(t) curve, the following device parameters are obtained: device capacitance, R_s, current bump initiation voltage, and R_p. The device capacitance is the total capacitance of the OLED; it may be used to estimate the total thickness of the OLED, if the permittivity is known. For the organic materials used in OLEDs the relative permittivity is typically 4 and the device capacitance is typically 30 nF/cm^2. The series resistance is estimated from the linear portion of the forward bias portion of the i(t)-v(t) curve. It is most likely due to bulk resistance of the constituent organic layers and it is generally not important at low applied voltages (< 10 V) since only a small amount of voltage drops across it at low current levels. The parallel resistance is typically not important for OLEDs but it is important for PLEDs

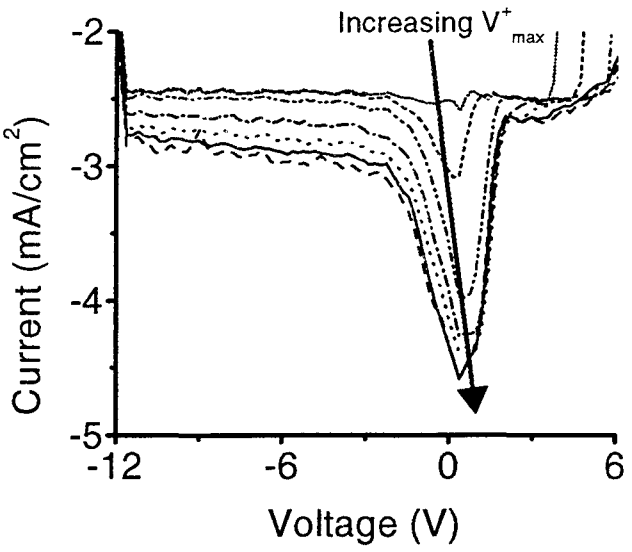

Figure 4.2. The bump portion of i(t)-v(t) curves with V^+_{max}=12, 10, 8, 7, 6, 5, and 4, respectively. As V^+_{max} is increased, the magnitude of the bump increases and then approximately saturates for V^+_{max}'s greater than approximately 8 V.

(see Section 4.5.2). The parallel resistance represents leakage of charge through the PLED below the threshold voltage.

A bump is observed during the downward ramping portion of the i(t)-v(t) curve, beginning at a forward voltage of about 2 V, as shown in Fig. 3.4. This bump was initially attributed to detrapping of electrons in the ETL; further analysis revealed that it is more likely caused by both the detrapping of charge in the ETL and the release of holes that accumulate at the ETL/HTL interface. A device physics analysis of current bump trends is presented in Section 4.4.

The current bump is strongly related to the forward bias parameters (*e.g.* V^+_{max} and PW^+). The bump increases in magnitude and then approximately saturates as V^+_{max} is increased, as shown in Fig. 4.2. This trend is ascribed to hole accumulation at the ETL/HTL interface. Hole accumulation at the ETL/HTL interface is expected to increase with increasing V^+_{max}, just as the charge stored on a parallel plate capacitor would increase with increasing applied voltage. The current bump increases with increasing V^+_{max} as long as more holes accumulate at the ETL/HTL interface with

increasing V^+_{max}. Saturation of the current bump is likely caused by a saturation in the concentration of holes accumulated at the ETL/HTL interface. This saturation in hole accumulation is expected to occur at large applied biases since hole accumulation results in a larger voltage drop across the ETL so that holes are injected into the ETL and recombine with electrons, as opposed to accumulating at the ETL/HTL interface (*i.e.* the injection of holes and electrons into the OLED is balanced).

Detrapping of electrons in the ETL may also be partially responsible for the current bump, although this is likely to be of secondary importance. Assuming that the area of the current bump is related to detrapped charge, increasing the number of trapped electrons in the ETL with increasing V^+_{max} is consistent with observed trends in which the area of the current bump increases with increasing V^+_{max}. Also, electrons released from traps during the current bump portion of the i(t)-v(t) curve are likely emitted from deeper traps, as electrons in shallow traps would be released before the current bump initiates. The release of trapped electrons from deep traps is expected to occur through a Frenkel-Poole mechanism and, thus, would be field-dependent. [37] Thus, detrapping current would likely occur at large negative biases. Electron detrapping may be partially responsible for the tail of the bump that extends to large reverse biases, as shown in Fig. 4.2.

The current bump is strongly dependent on PW^+ for small V^+_{max}'s, as shown in Fig. 4.3. At large V^+_{max}'s, the PW^+ dependence is not as strong. The relation between PW^+, V^+_{max}, and the magnitude of the current bump is best shown with a $Q_{detrapped}$-PW^+ plot, as presented in Fig. 3.8. At small applied biases, few holes are injected into the HTL and it takes a long time relative to the time of the forward bias portion of the applied voltage waveform for holes to accumulate at the ETL/HTL interface. At large applied biases, many holes are injected into the OLED and accumulate at the ETL/HTL interface. Notice that this is equivalent to modeling the HTL as a variable resistance in which the resistance of the HTL is large at low voltages and small at high voltages. If the ETL is modeled as a capacitor, the RC time constant of the ETL/HTL layers is large at small applied voltages and small at large applied voltages.

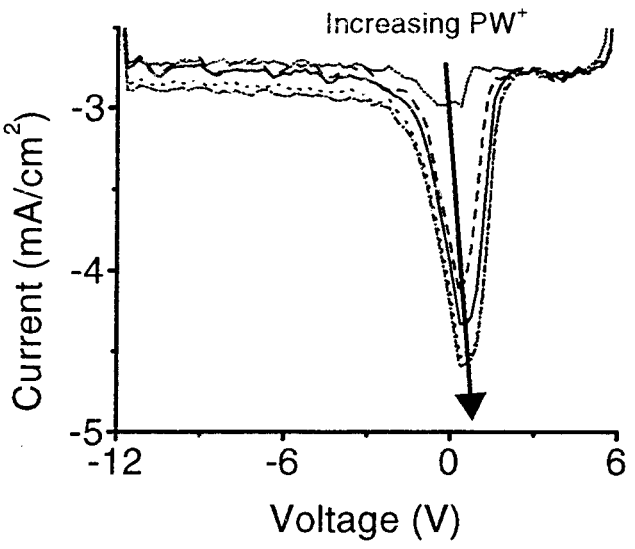

Figure 4.3. The bump portion of i(t)-v(t) curves with $V^{+}_{max} = 6$ V and PW^{+}=1000, 600, 200, 100, and 0, respectively. The bump increases in magnitude and the approximately saturates for $PW^{+} > 600$ μs.

The current bump has little dependence on PW^{-}, D, and V^{-}_{max}, so that these curves are not shown. Most of the charge stored at the ETL/HTL interface quickly exits the device when the voltage is ramped down to a small enough voltage. It is this charge that exits the OLED when the bias is below ~ 2 V that is believed to be responsible for the current bump.

The forward bias portion of an i(t)-v(t) curve is also strongly dependent on waveform parameters. In general, the OLED turns on harder if V^{+}_{max} and PW^{+} are large and softer if V^{-}_{max}, PW^{-}, and D are large. Note that harder [softer] turn on means that the current is larger [smaller] at a given voltage. The V^{+}_{max} and PW^{+} dependencies are shown in Figs. 4.4 and 4.5, respectively. The i(t)-v(t) dependence on PW^{-}, D and V^{-}_{max} are not shown due to the weak dependence on these parameters. These trends are explained by hole accumulation at the ETL/HTL interface. A large hole accumulation at the ETL/HTL interface results in a greater voltage drop across the ETL at given forward bias voltage, as discussed in Section 4.4. A greater voltage drop across the ETL aids electron injection into the ETL and the balance of electron

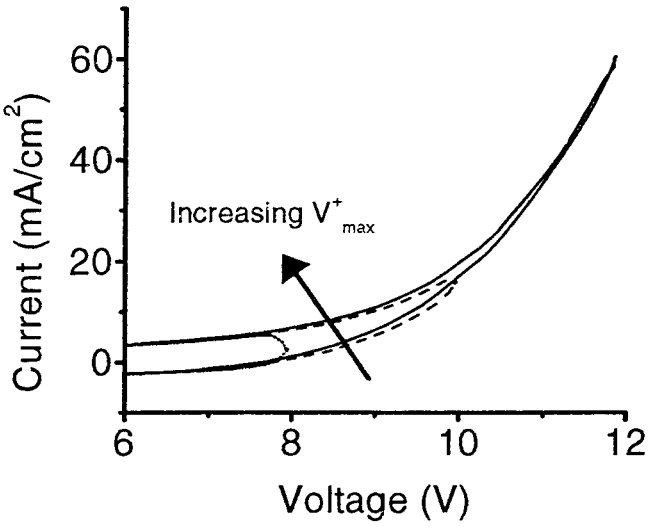

Figure 4.4. The forward bias portion of i(t)-v(t) curves with V^+_{max}=12, 10, and 8 V. The OLED turns on harder with increasing V^+_{max}.

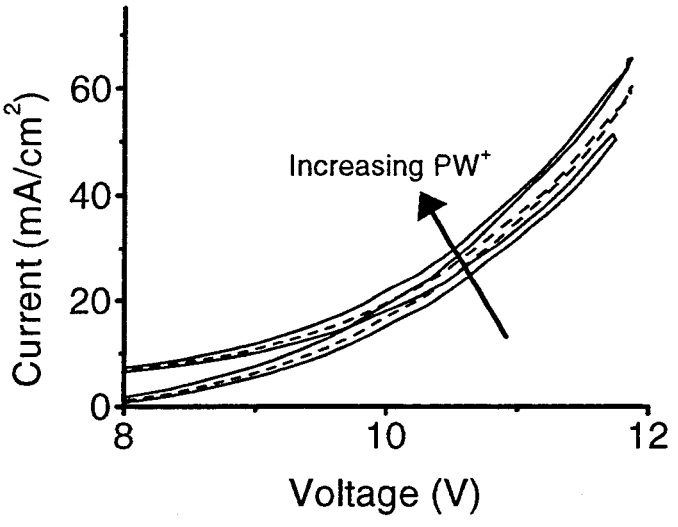

Figure 4.5. The forward bias portion of i(t)-v(t) curves with PW^+=1000, 200, and 0 μs. The OLED turns on harder as PW^+ is increased.

and hole injection into the ETL is improved. Thus, when V^{+}_{max} and PW^{+} are large, more holes are able to build up at the ETL/HTL interface and enhance conduction, causing the OLED to turn on harder. Notice that this explanation implies that some holes remain at the ETL/HTL interface throughout the negative bias portion of the waveform and that the amount of charge that remains is dependent on the amount of charge that accumulates during the forward bias portion of the waveform. For large PW^{-}, V^{-}_{max}, and D more holes are extracted from the ETL/HTL interface during the negative bias portion of the applied voltage waveform and the OLED turns on softer.

4.3.2 Steady-State Transient Brightness-Transient Current Analysis

Steady-state transient brightness-transient current [b(t)-i(t)] analysis has proven to be one of the most useful methods developed in this thesis. This method is most useful when a DC B-I curve is compared to an AC b(t)-i(t) curve, as discussed in Chapter 3. The key assumption implicit in this analysis is that ETL current and brightness are directly proportional. This is a good assumption as long as few of the holes injected from the anode reach the cathode, and ETL conduction current due to trapping is small. [34, 35] Very few holes are likely to make it clear across the ETL without recombining. However, if the injection of holes and electrons is extremely mismatched, accumulation of holes at the ETL/HTL interface could be come excessive so that some holes may transport across the ETL without recombining. Notice that brightness is proportional to the ETL conduction current (*i.e.* i^{c}_{ETL}), not to displacement or trapping current (*i.e.* i^{t}_{ETL}).

A typical b(t)-i(t)/B-I plot is shown in Fig. 4.6. The important thing to notice about Fig. 4.6 is that $i^{+}_{offset}(t)$ is significantly larger than the $i^{-}_{offset}(t)$. The $i^{+}_{offset}(t)$ is approximately twice that of $i^{-}_{offset}(t)$. There are two possible explanations for this difference in the magnitude of the offsets: (1) there is a large i^{t}_{ETL} current component during the positive ramp that is not present during the negative ramp, or (2) the ETL displacement current is greater during the positive ramp than it is during negative

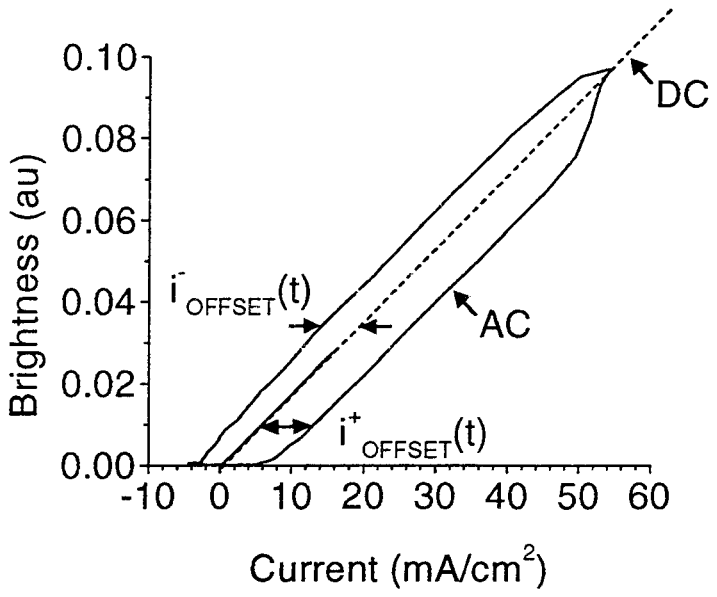

Figure 4.6. b(t)-i(t)/B-I curves indicated by AC and DC, respectively. The dotted line is an extrapolation of the B-I curve to larger currents. Notice that $i^-_{offset} \approx 4$ mA/cm^2 and $i^+_{offset} \approx 8$ mA/cm^2.

ramp. It is unlikely that the i^t_{ETL} is constant during the forward voltage ramp because as empty traps fill the trapping current is expected to decrease. Thus, explanation (1) is probably not correct and explanation (2) seems more likely, as discussed in the following. This experiment is the best evidence that accumulation at the ETL/HTL interface is more important to OLED operation than electron trapping in the ETL.

If during the positive voltage ramp holes are easily injected into and transported across the HTL, the HTL is effectively shunted, and the measured capacitance is due exclusively to the ETL capacitance. However, during the negative voltage ramp holes that accumulate at the ETL/HTL interface are unable to exit the OLED as the voltage decreases, so that the injection of electrons and holes are approximately balanced due to the hole accumulation at the ETL/HTL interface. Thus, i_{ETL} is equal to i_{HTL}, implying $C_{ETL}\frac{dv_{ETL}}{dt} = C_{HTL}\frac{dv_{HTL}}{dt} = C_t\frac{dv}{dt}$, and the measured negative voltage ramp capacitance is that of the entire OLED stack. Therefore, the ETL capacitance, C_{ETL}, the capacitance of the entire OLED stack, C_t, and the HTL capacitance, C_{HTL}, can be estimated from b(t)-i(t)/B-I analysis using the following

equations:

$$C_{ETL} = \frac{I^{+}_{offset}}{\frac{dv}{dt}\mid_{+Ramp}}, \tag{4.1}$$

$$C_t = \frac{I^{-}_{offset}}{\frac{dv}{dt}\mid_{-Ramp}}, \tag{4.2}$$

and

$$1/C_{HTL} = 1/C_t - 1/C_{ETL}. \tag{4.3}$$

The thickness of the ETL and HTL may be calculated from the respective capacitance via d=$\frac{\epsilon A}{C}$. This provides a method for estimating the thickness of the ETL and HTL.

In summary the main assumptions necessary to extract C_{ETL}, C_{HTL}, and C_t from b(t)-i(t)/B-I curves are: (1) b(t) is proportional to i^{c}_{ETL}(t) by α, (2) i^{t}_{ETL}(t) is negligible, (3) during upward ramping portion of the applied voltage ramp the HTL behaves primarily as a resistor and the ETL behaves primarily as a capacitor so that $\frac{dv(t)}{dt} \approx \frac{dv_{ETL}(t)}{dt}$, and (4) during the downward ramping portion of the applied voltage ramp i_{ETL}(t) $\approx$ i_{HTL}(t) so that $C_{ETL}\frac{dv_{ETL}}{dt} \approx C_{HTL}\frac{dv_{HTL}}{dt} \approx C_t\frac{dv}{dt}$. (1) and (2) are likely to be approximately true based on the behavior of the b(t)-i(t) curve. (3) and (4) appear to be good assumptions based on the device physics operation of OLEDs, as discussed in Section 4.4.

From Fig. 4.6 it is observed that i^{+}_{offset} is approximately 8 mA/cm^2 and i^{-}_{offset} is approximately 4 mA/cm^2 (i^{-}_{offset} could be estimate between 3 and 4 mA/cm^2). Notice that i^{-}_{offset} is a rough estimate and there is some ambiguity in the value of i^{-}_{offset}. From Eqs. 4.1, 4.2, and 4.3 the capacitances 80, 40, and 80 nF/cm^2 are found for C_{ETL}, C_t, and C_{HTL}, respectively. However, from the below-threshold portion of the i(t)-v(t) curve shown in Fig. 3.4, the total OLED capacitance is found to be about 30 nF/cm^2. Thus, b(t)-i(t) analysis does not provide exact values of C_t and should be used for comparing the relative thicknesses of the ETL and HTL. Assuming a relative permittivity of 4 for both the ETL and HTL, the thicknesses of the ETL (d_{ETL}), the entire OLED stack (d_{OLED}), and the HTL (d_{HTL}) are estimated to be 443, 885, and 443 Å, respectively.

4.3.3 Steady-State Transient Brightness-Transient Voltage Analysis

The viability of steady-state transient brightness-transient voltage [b(t)-v(t)] analysis depends on the validity of the assumption that the conduction current and brightness are directly proportional. If this assumption is made, it is clear that b(t)-v(t) trends are identical to the trends that would be observed in an i_{ETL}(t)-v(t) curve, if such a curve could be generated. Note that generating an i^c_{ETL}(t)-v(t) curve from an i(t)-v(t) curve is a daunting task since it is difficult to unambiguously extract i_{ETL}(t) from i(t).

b(t)-v(t) curves have counterclockwise hysteresis, as shown in Fig. 4.7. This trend is best explained as due to a larger accumulation of holes at the ETL/HTL interface during the negative voltage ramp than during the positive voltage ramp. Radiative recombination and conduction are enhanced by the accumulation of holes at the ETL/HTL interface, due to balanced hole and electron injection into the ETL. Another mechanism that could contribute to the counterclockwise hysteresis is electron trapping in the ETL. During the positive voltage ramp, most of the electrons first injected into the ETL are trapped and do not contribute to the conduction current. During the negative voltage ramp, most of the electron traps are filled so that all injected electrons contribute to conduction current. Thus, the trapping and detrapping of electrons in the ETL may play a role in establishing the hysteretic nature of the b(t)-v(t) curve.

The b(t)-v(t) curve turns on harder with larger values of V^+_{max} and PW^+ and softer with larger values of V^-_{max}, PW^-, and D. b(t)-v(t) curves showing a harder turn on with increasing V^+_{max} and PW^+ are shown in Figs. 4.7 and 4.8, respectively. Figures are not shown for increasing V^-_{max}, PW^-, and D because these changes are very small. Since conduction current and brightness are proportional, a harder turn on of the i(t)-v(t) curve results in a concomitant harder turn on of the corresponding b(t)-v(t) curve. Thus, increased hole accumulation at the ETL/HTL interface results in a harder turn on of the b(t)-v(t) curve, just as it does with a i(t)-v(t) curve. Increasing V^+_{max} and PW^+ allows more holes to accumulate at the ETL/HTL

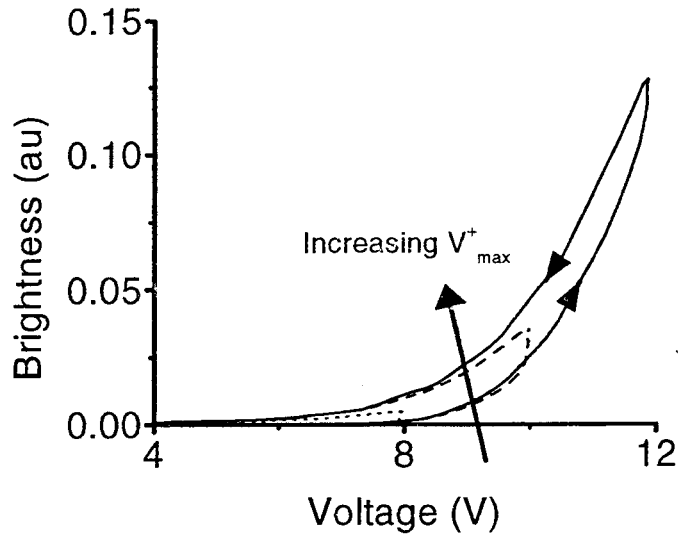

Figure 4.7. b(t)-v(t) curves with V^{+}_{max}=12, 10, and 8 V, respectively. The b(t)-v(t) curve turns on harder with increasing V^{+}_{max}. Also, the b(t)-v(t) curve has counter-clockwise hysteresis as indicated by the arrows.

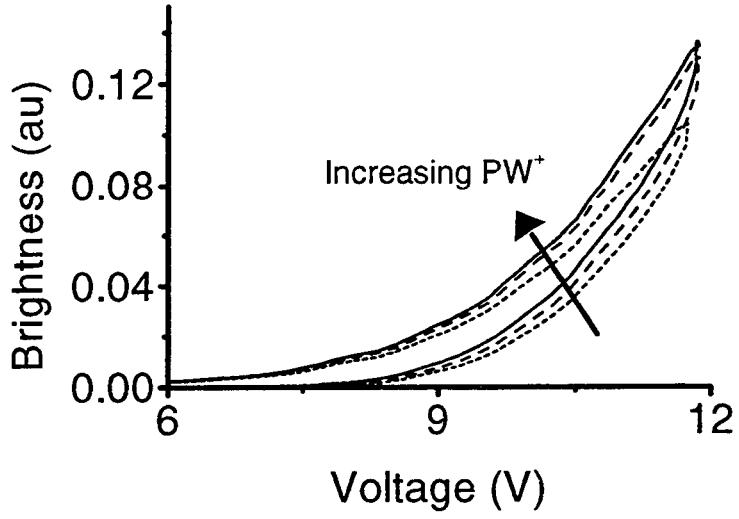

Figure 4.8. b(t)-v(t) curves with PW^{+}=1000, 200, and 0 μs, respectively. The b(t)-v(t) curve turns on harder as PW^{+} is increased.

interface so that the OLED turns on harder. Increasing V^{-}_{max} and PW^{-} allows for more removal of holes at the ETL/HTL interface and the OLED turns on softer.

4.3.4 Transient Voltage, Current, and Brightness Analysis

Transient voltage, current, and brightness plots often reveal information that is not apparent in an i(t)-v(t) curve. The i(t)-v(t) curve does not provide much information about what occurs during the plateau portions of the applied voltage waveform. Also, it does not directly indicate how the current or voltage change with time.

Plots showing the plateau portion of the current transient and brightness transient for various V^{+}_{max}'s are given in Figs. 4.9 and 4.10, respectively. For small V^{+}_{max}, the current decreases during the plateau portion of the applied voltage waveform. For large V^{+}_{max}, the current increases during the voltage plateau. However, the brightness always increases or is constant during the voltage plateau. The transition from a decreasing current to an increasing current during the plateau portion of the current transient as V^{+}_{max} is increased is explained by a transition from $C_{ETL}\frac{dv_{ETL}}{dt}$ and i^{t}_{ETL}-dominated current to $i^{c}_{ETL}(t)$-dominated current. As traps fill and holes at the ETL/HTL interface accumulate, the current components $C_{ETL}\frac{dv_{ETL}}{dt}$ and $i^{t}_{E}TL(t)$ decrease, while $i^{c}_{ETL}(t)$ increases for a constant voltage. At about $V^{+}_{max} = 8$ V the plateau current transitions from increasing to to decreasing. The brightness transient always increases during the voltage plateau because $i_{ETL}(t)$ is increasing.

4.3.5 Brightness Bump

A small brightness bump is observed in both the brightness transient and b(t)-v(t) curves for some OLEDs when the PMT gain is large, as shown in Figs. 4.10 and 4.11, respectively. Notice that the brightness bump occurs after the current bump and at more negative voltages. The brightness bump minimum occurs near the current bump maximum and the brightness bump maximum typically occurs just after the current bump, as shown in Fig. 4.11. The magnitude of the brightness bump increases

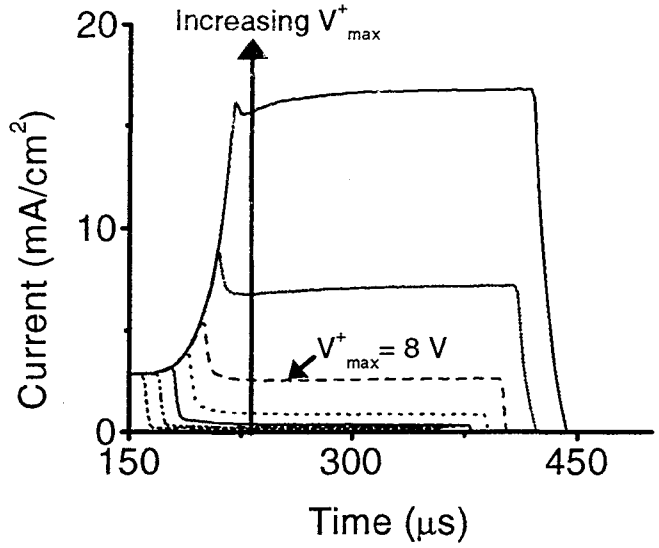

Figure 4.9. The applied voltage plateau portion of the current transient with V^{+}_{max}=10, 9, 8, 7, 6, 5, and 4 V, respectively. Notice that for V^{+}_{max} greater than approximately 8 V the current transient in the latter portion of the voltage pulse changes from decreasing to increasing.

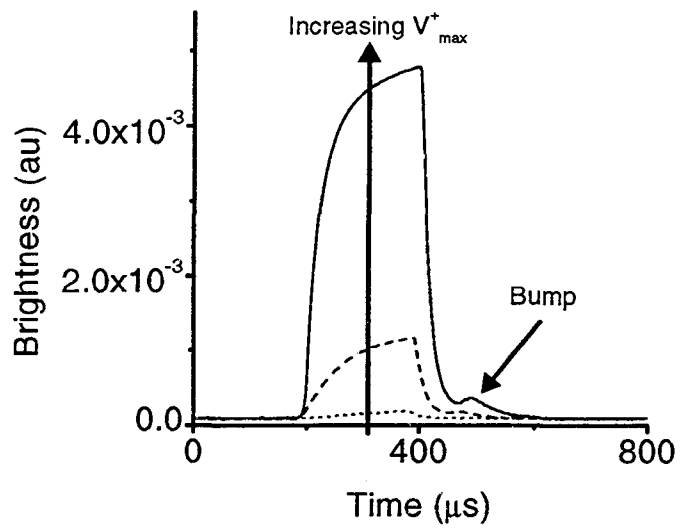

Figure 4.10. The applied voltage plateau portion of the brightness transient for V^{+}_{max}=8, 7, and 6 V, respectively. Notice that a brightness bump follows the forward bias brightness transient. Also, note that the brightness increases during the forward bias applied voltage plateau.

as V^{+}_{max} increases until a maximum brightness is reached and then the brightness bump decreases in magnitude as V^{+}_{max} is increased, as shown in Fig. 4.11.

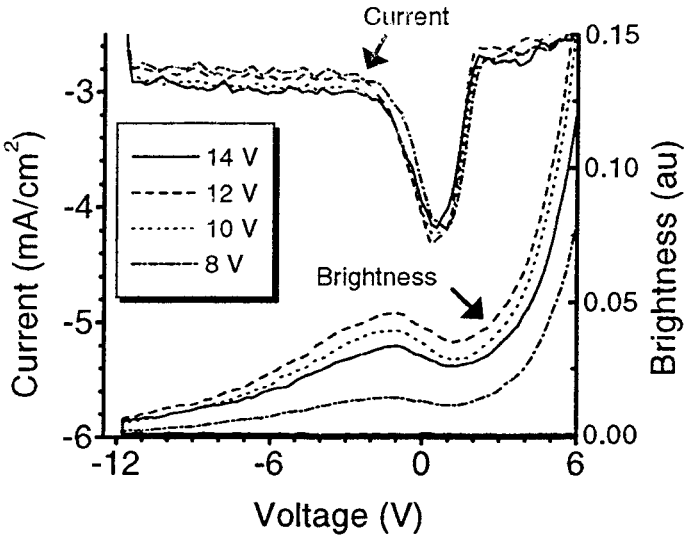

Figure 4.11. The bump portion of b(t)-v(t) and i(t)-v(t) curves for V^{+}_{max}=14, 12, 10, and 8 V, respectively. The i(t)-v(t) curves are toward the top of the plot while the b(t)-v(t) curves are toward the bottom. Notice that both of these curves are obtained during the negative voltage ramp so that the brightness bump occurs after the current bump and the maximum of the current bump magnitude occurs near the brightness bump minimum.

By spectrally resolving the light output using a monochrometer, the brightness bump is shown to peak at the same wavelength as the light output during the forward bias portion of the applied voltage waveform. This indicates that the brightness bump is caused by the same luminescent center as the brightness that occurs during the forward bias portion of the applied voltage waveform. Thus, the brightness bump originates from recombination of holes and electrons in the ETL.

The best explanation for the brightness bump involves the existence of an electric dipole at the ETL/HTL interface. The brightness bump occurs due to the mutual attraction of holes and electrons near the ETL/HTL interface region after the field within the OLED is zero or negative. The field within the OLED is approximately zero only after the applied voltage is below the flat-band voltage (~1.1 V) and some

of the holes at the ETL/HTL interface have begun to be removed. Notice that this explanation requires that holes and electrons are able to move past each other during the forward bias portion of the applied voltage waveform. It may be possible that some of holes injected into the ETL are trapped and the dipole is between these trapped holes and electrons that have been trapped or accumulated near the ETL/HTL interface. Although Nikitenko *et al.* used a very different OLED structure than that used in this thesis, they have observed a similar brightness overshoot and have attributed it to an interface region at the ETL/HTL interface. [38] Nikitenko *et al.* also found that the brightness overshoot is related to how the OLED is manufactured. Although the brightness bump is most likely caused by a dipole of some kind near the HTL/ETL interface, a more detailed explanation will likely require a more complete understanding of OLED structure and manufacturing methods.

4.3.6 Detrapped Charge Analysis

Detrapped charge analysis is helpful in determining how charge is accumulated and trapped within the OLED. Also, it is the best way to view the relation between various waveform parameters and the magnitude of the current bump. A $Q_{detrapped}$-$Q_{transferred}$ plot, as shown in Fig. 4.12, reveals that when a small amount charge is transferred, the transferred charge and detrapped charge are approximately equal. When a large amount of charge is transferred, the transferred charge is much greater than the detrapped charge. This implies that when little charge is transferred the transferred charge is almost entirely made up of charge that is accumulated or trapped. This is a very similar result to that obtained from the current transient analysis described in Section 4.3.4. Notice that this effect is similar to the way a capacitor charges up through a series resistor.

A $Q_{detrapped}$-PW^+ plot is helpful in understanding how charge accumulates and is released from the OLED with time. A $Q_{detrapped}$-PW^+ plot is shown in Fig. 4.13. A larger PW^+ allows more time for charge accumulation within the OLED and more charge is released during the bump portion of the applied voltage waveform. Changes

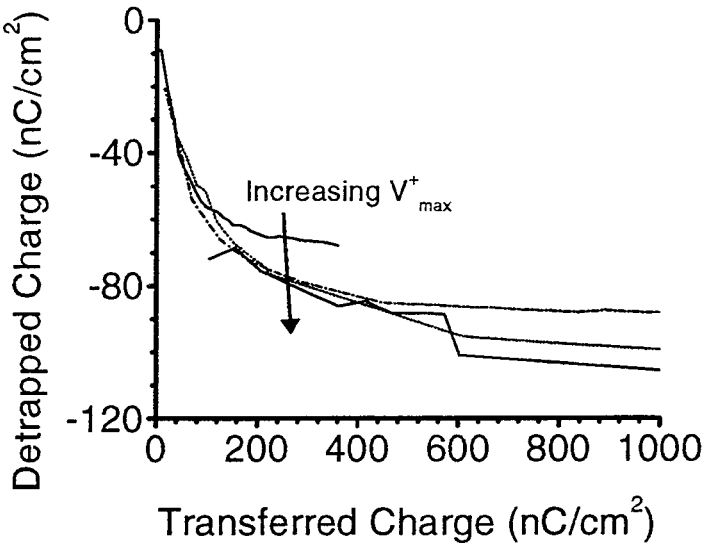

Figure 4.12. A representative set of $Q_{detrapped}$-$Q_{transferred}$ curves with V^+_{max}= 6, 7, 8, and 9 V, respectively. The arrow indicates increasing V^+_{max}. In the initial presaturation portion of the curve, the magnitude of $Q_{detrapped}$ is approximately equal to the magnitude of $Q_{transferred}$.

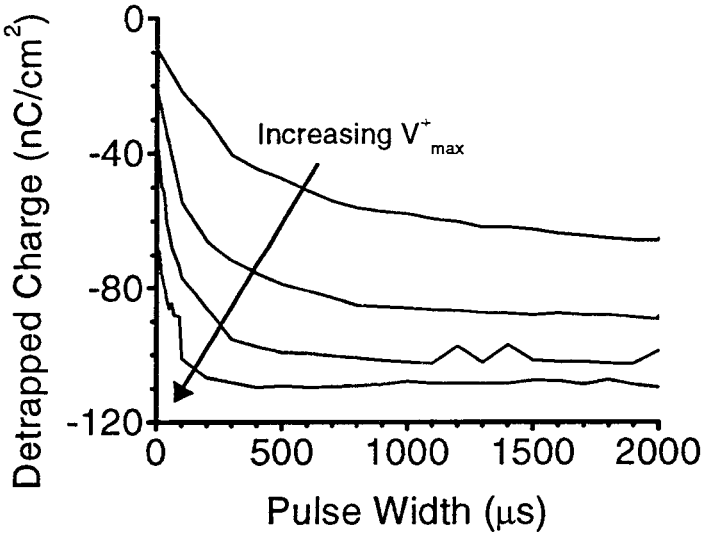

Figure 4.13. A representative set of $Q_{detrapped}$-PW$^+$ curves with V^+_{max}= 6, 7, 8, and 9 V, respectively. The arrow indicates increasing V^+_{max}. Note that decreasing $Q_{detrapped}$ indicates that more accumulated and/or trapped charge is released; the detrapped current is negative, so the polarity of the detrapping charge is negative. The $Q_{detrapped}$ saturation magnitude increases with increasing V^+_{max}.

in the bump with increasing PW^+ are shown in Fig. 4.3. In the $Q_{detrapped}$-PW^+ plot shown in Fig. 4.13 the magnitude of the bump increases and then saturates as PW^+ is increased. Also, notice that at larger V^+_{max}'s the bump saturates for much smaller PW^+'s.

The time constant that characterizes the accumulation of charge decreases as V^+_{max} is increased. Effectively, the resistance through the HTL decreases as voltage increases and the corresponding RC time constant decreases. The resistance of the HTL would be expected to decrease as the voltage drop across it increases for both the case of bulk-limited and injection-limited conduction across the HTL. For the case of bulk-limited conduction, space-charge-limited and trap-charge-limited conduction may be likely conduction mechanisms; they are both strongly field-dependent. Injection-limited conduction is field-dependent due to barrier-lowering.

4.4 OLED Device Physics Modeling

This section summarizes the devices physics modeling employed in this thesis. Notice that this model is somewhat similar to the device physics model developed by Khramtchenkov *et al.* [34, 35] However, in the model presented here, the effects of charge trapping in the ETL are explored. Also, bulk-limited transport and capacitive effects are discussed herein. The model consists of assuming that the OLED operates via electron injection from the cathode into the ETL and hole injection into the HTL, with recombination occurring in the ETL near the ETL/HTL interface. This thesis provides experimental evidence that hole accumulation and electron trapping play an important role in determining the characteristics of OLEDs.

Evidence presented in this thesis suggests that hole accumulation occurs at the HTL side of the ETL/HTL interface. This evidence derives directly from displacement currents measured during the forward bias portion of the applied voltage waveform obtained from b(t)-i(t) curves. This accumulation of charge is believed to be due to hole accumulation at the HTL side of the ETL/HTL interface, as opposed to electron accumulation at the ETL side of the ETL/HTL interface, because the

injection barrier for holes at the anode is much smaller than the injection barrier for electrons at the cathode. Also, the mobility of holes in the HTL is much larger (about 1000 times) than the mobility for electrons in the ETL, as discussed in Chapter 2. Thus, the ETL is more insulator-like than the HTL. Conduction in an OLED is expected to be injection-limited at the cathode or bulk-limited in the ETL. Alternatively, if conduction were limited by injection from the cathode or the ETL bulk, hole charge would accumulate across the HTL. At large applied voltages, the ETL begins to conduct charge and further hole accumulation decreases sharply. This corresponds to the voltage at which the current bump saturates.

Charge trapping may also be partially responsible for some of the observations discussed in this thesis. For example, the current bump may in part be caused by trapping of electrons in the ETL. For trapping to contribute to the bump, the emission rate of electrons from traps must be relatively low (*i.e.* the amount of trapped charge does not quickly adjust when the applied voltage is changed). If the emission rate is large, trapped charge would quickly be released as the applied voltage is decreased. Also, the release of trapped charge may be voltage-dependent via a Frenkel-Poole emission mechanism. In this case more charge would be released from traps at large negative voltages. In an i(t)-v(t) curve, this would be observed as a decreasing negative current during the negative bias, negative ramping portion of the applied voltage waveform. This feature is sometimes observed in i(t)-v(t) curves.

Trapping of electrons in the ETL should have an effect on the injection and transport of charge through the ETL. If trapping in the ETL is a dominant effect, the current transient curve would decrease during the plateau portion of the applied voltage waveform, even for large V^{+}_{max}'s. This would indicate that an increasing build up of space charge is inhibiting the current flow. However, evidence of significant trapping is not observed in the i(t) transient since the current transient increases above the saturation voltage during the plateau portion of the waveform. Electron trapping in the ETL may be partly responsible for reversible aging, as discussed Chapter 5.

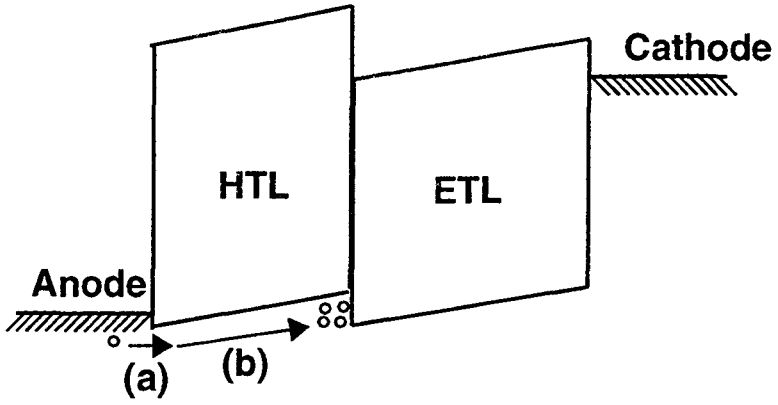

Figure 4.14. An energy band diagram of an OLED at a voltage just large enough to inject holes into the HTL. (a) Holes are injected into the HTL. (b) Holes transport across the HTL and accumulate at the ETL/HTL interface.

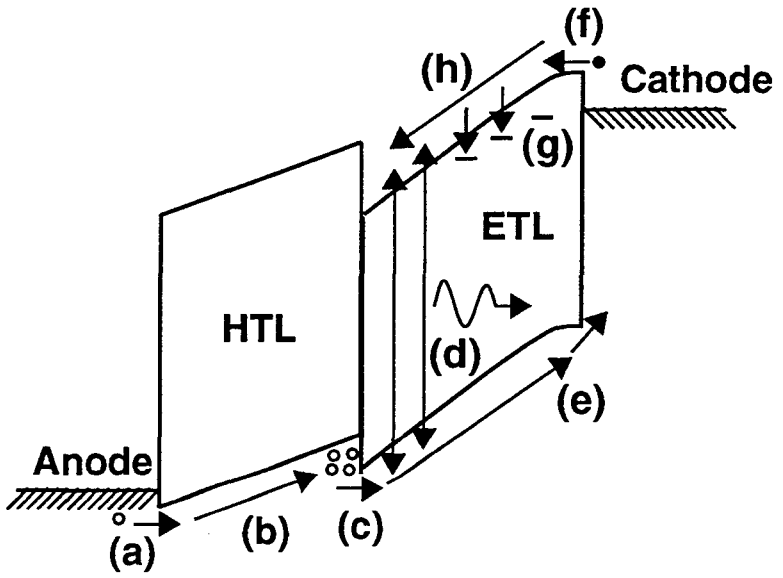

Figure 4.15. An energy band diagram of an OLED during the positive forward biased voltage ramp. (a) Holes are injected from the anode into the HTL and (b) they transport across the HTL. (c) At the HTL/ETL interface the holes accumulate and some are injected into the ETL. (d) Holes recombine with electrons over a wide recombination zone producing light. (e) Some holes transport through the ETL and exit through the cathode. (f) Electrons are injected into the ETL, (g) some are trapped in the ETL, and (h) the remaining are transported across the ETL.

The following is a description of the OLED physics as it is subjected to the applied voltage waveform discussed in this thesis. Notice that there are differences between this model and the model discussed in Chapter 2. During the positive ramping portion of the applied voltage waveform, holes begin to be injected from the anode at a voltage near the threshold voltage, as shown in Fig. 4.14. During this early stage of the positive voltage ramp, holes begin to accumulate at the HTL/ETL interface and very few holes are injected into the HTL. Also, few if any electrons are injected into the ETL. At this voltage the HTL behaves primarily as a voltage-dependent resistor and the ETL behaves as capacitor.

As the voltage is ramped up to a voltage above V_t, electrons begin to be injected into the ETL, as shown in Fig. 4.15. Some of the injected electrons are trapped in the ETL and the injection of electrons and holes is still mismatched. Holes continue to accumulate at the ETL/HTL interface and a few are injected into the ETL. If the number of electrons being injected into the ETL is smaller than the number of holes being injected into the ETL, there may be a hole leakage current. At this applied voltage the emission zone in the ETL is relatively wide due to the mismatch of carrier injection into the ETL. [17] Also, during this portion of the applied voltage waveform the ETL behaves as a leaky capacitor and the HTL behaves as a voltage-dependent resistor.

As the voltage is ramped up to the positive plateau portion of the applied voltage waveform, the electron and hole injection into the ETL and HTL, respectively, improves and becomes balanced, as shown in Fig. 4.16. At this applied voltage, electrons are able to transport across the ETL much more efficiently and most holes injected into the HTL are subsequently injected into the ETL after being transported across the HTL. Thus, the HTL and ETL both behave as voltage dependent resistors. Notice that there is more voltage dropped across the ETL than across the HTL due to hole accumulation at the ETL/HTL interface and hole and electron injection into the ETL is balanced. Holes are no longer able to leak through the ETL without recombining with an electron due to well matched injection of electrons and holes. The emission zone in the ETL at which electron-hole pair recombination occurs is

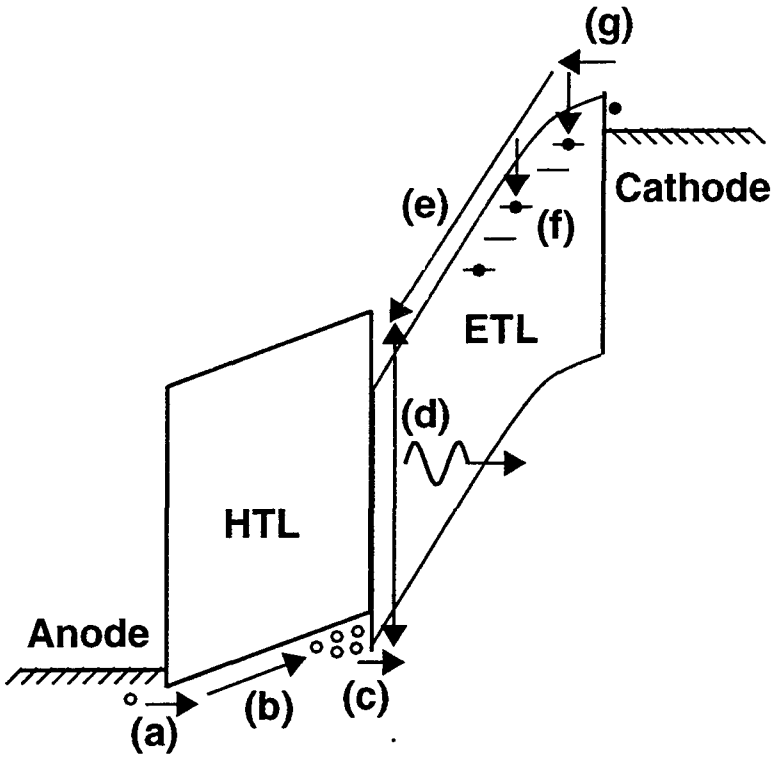

Figure 4.16. An energy band diagram of an OLED at a large forward bias. (a) Holes are injected from the anode into the HTL and (b) they transport across the HTL. (c) Holes are injected from the HTL into the ETL and (d) they recombine with electrons producing light. (e) Electrons transport across the ETL. (f) Some electrons are trapped in the ETL. (g) Electrons are injected from the cathode into the ETL.

very narrow at this applied voltage. [17] Also, notice that electron trapping in the ETL near the cathode has bent the bands, inhibiting electron injection. During the plateau portion of the applied voltage waveform, the accumulation of holes at the ETL/HTL interface reaches a steady-state with the applied voltage.

As the voltage is ramped down but still above the threshold voltage, few holes are able to leave the ETL/HTL interface. The holes at the ETL/HTL interface can only leave the OLED by injection into the ETL and recombination there with electrons. However, if holes are removed from the ETL/HTL interface the injection of electrons and holes into the ETL is no longer balanced, Thus, the hole removed will be quickly replaced. Notice that because the accumulated hole charge at the ETL/HTL interface cannot adjust to the changing applied bias, the capacitance is

essentially that of the entire OLED. The hole charge remaining at the ETL/HTL interface is responsible for improved electron injection during the negative ramp, accounting for the hysteresis of the b(t)-v(t) curve.

As the voltage is ramped downward below the V_t, electrons and holes are no longer able to be injected from the cathode and anode, respectively. At roughly V_I, most of the voltage is dropped across the ETL and the holes at the ETL/HTL interface are able to exit through the anode, as shown in Fig. 4.17. Holes exiting through the anode account for the bump observed in an i(t)-v(t) curve.

As the voltage is ramped to small negative voltages (< -2V), electrons trapped within the ETL may be released from traps via field emission, as shown in Fig. 4.18. Notice that electron detrapping in the ETL may be responsible for the tail portion of the current bump, which extends to large negative voltages. Only electrons in relatively deep traps could be responsible for this because electrons in shallower traps would be released at smaller voltages.

During the negative plateau and positive ramping portion of the applied voltage waveform electrons and holes continue to be removed from the OLED. As the waveform continues, the energy bands returns to that of Fig. 4.15.

4.5 Device Comparison

In this thesis four types of OLEDs are investigated: two types of small-molecule green OLEDs, PLEDs, and small molecule blue OLEDs. Primarily the small molecule green OLED is investigated in this thesis and the blue OLED and PLED are used for comparison. The blue OLED is believed to be comprised of a different ETL material than that used in the green OLED. Other than this, the structural differences between the OLED samples tested are unknown. The PLED is essentially a single layer device and it is used as a comparison to the organic heterojunction of the OLEDs. The experimental results of the blue OLED and both types of green OLED are summarized at the end of this section in Table 4.1.

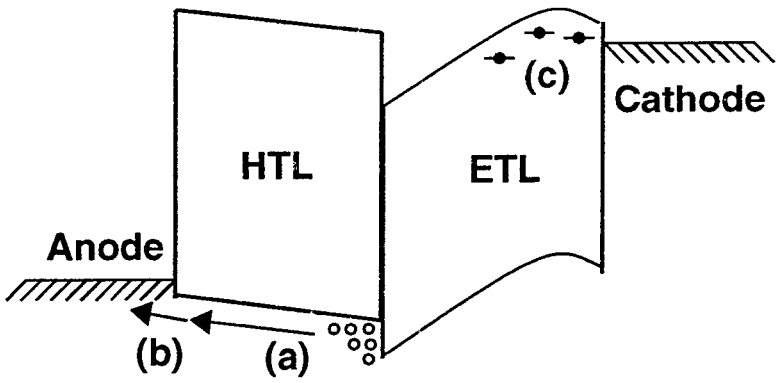

Figure 4.17. An energy band diagram of an OLED at a voltage sufficiently small to initiate the current bump. (a) Holes that have accumulated at the ETL/HTL interface transport across the HTL and (b) exit through the anode. (c) Some electrons remain trapped in the ETL.

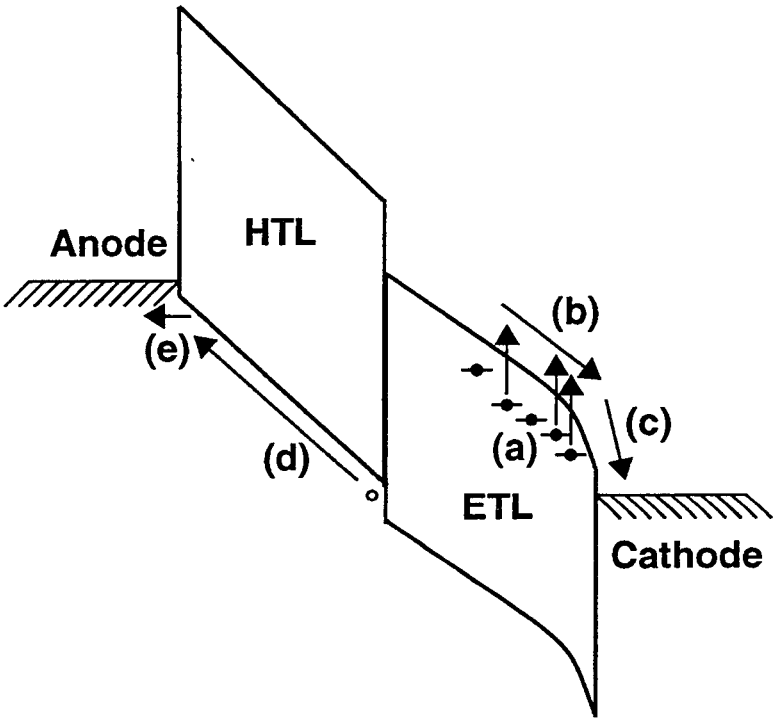

Figure 4.18. An energy band diagram of an OLED at a large negative voltage. (a) Electrons detrap from the ETL, (b) transport across the ETL, and (c) exit through the cathode. (d) Some holes still remain at the HTL/ETL interface and transport across the HTL. (e) Holes exit through the anode.

4.5.1 Blue OLED Versus Green OLEDs

The i(t)-v(t) curves of a typical blue OLED and a typical green OLED with the same device area are shown in Fig. 4.19. The blue OLED is not nearly as bright at a given forward voltage as the green OLED. The blue OLED forward bias i(t)-v(t) characteristic is shifted about 2 V higher than that of the green OLED. Also, V_I is 4 V for the blue OLED and 2 V for the green OLED. One possible explanation for these voltage shifts between the blue and green OLEDs is a 2 V difference in the flat-band voltage. However, this explanation seems unreasonable since such a large flat band voltage would indicate drastically different OLED materials. A more likely explanation for this voltage shift is that the blue OLED possesses a thicker ETL. A thicker ETL would require the same field for charge to be injected and/or transported as a thinner ETL. Thus, a larger voltage drop would be required across a thick ETL compared to a thin ETL for the same ETL field. Therefore, a thicker ETL results in a larger threshold voltage. The area of the current bump is not appreciably different between the blue and the green OLED. Assuming that the ETL behaves as a capacitor the electric field, F, within the ETL is given by

$$F = \frac{Q}{\epsilon A}, \tag{4.4}$$

where Q is the charge stored across the ETL, ϵ is the permittivity, and A is the OLED area. Assuming that the permittivity and the area are the same for both the blue and the green OLED, then Q must be the same for both devices. Thus, the total number of holes that accumulate at the ETL/HTL interface is expected to be roughly the same for all ETL thicknesses. Also, a larger voltage drop across the ETL for an OLED with a thicker ETL to obtain the same charge and field across the ETL means that the bump initiates at a larger voltage. This analysis implies that the blue OLED is thicker than the green OLED, assuming that the permittivity of the ETL is the same for both the blue and green OLEDs.

Notice in Fig. 4.19 that the displacement current of the blue OLED below the threshold voltage is less than the displacement current of the green OLED, indicating that the blue OLED has a smaller total capacitance than the green OLED. Thus,

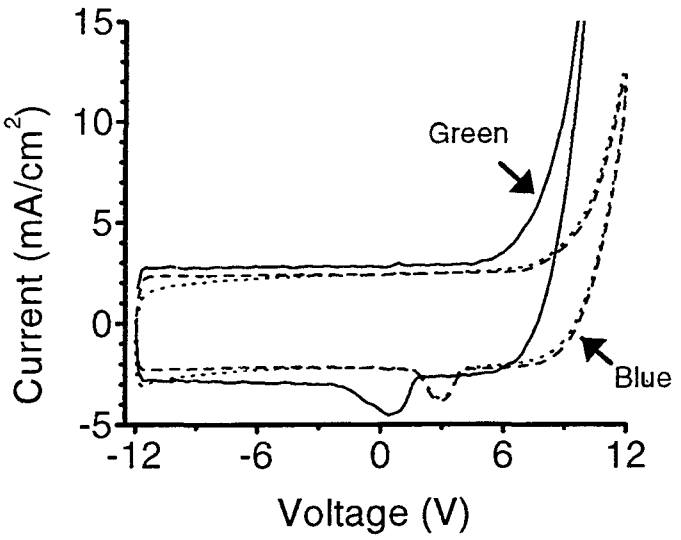

Figure 4.19. An i(t)-v(t) curve for a green OLED and two i(t)-v(t) curves for blue OLEDs from the same substrate. Notice that the green i(t)-v(t) curve goes off the scale. The bump for the blue OLED initiates at about 4 V while the bump for the green OLED initiates at about 2 V. Also, the displacement current for the green OLED is greater than that of the blue OLED.

this indicates that the blue OLED is thicker than the green OLED. This supports the hypothesis that the blue ETL is thicker than the green ETL.

Figure 4.19 shows that the magnitude of the current bump of the blue OLED is slightly smaller than that of the the green OLED. Since the magnitude of the current bump is related to Q and Q is expected to be the same for both devices, the areas of the current bumps are expected to be the same. A possible reason for their difference is that the blue ETL conducts electrons more easily than the green ETL. Thus, a lower field would be required to inject charge into the blue ETL compared to the green ETL and fewer holes would accumulate at the ETL/HTL interface. Alternatively, the effective areas of the OLEDs may be different due to the growth of dead spots (see Chapter 5).

Differences in ETL thicknesses of the blue and green OLED may be in part verified by the b(t)-i(t) curves, as shown in Fig. 4.20. The $i^{+}_{offset}(t)$ and $i^{-}_{offset}(t)$ of the blue OLED is 3.5 mA/cm^2 and 2.5 mA/cm^2, respectively (3.5 mA/cm^2 is an

average value for $i^{+}_{offset}(t)$). Thus, assuming that the relative permittivity is 4, d_{ETL}, d_{HTL}, and d_{OLED} of the blue OLED are 1011, 405, and 1416 Å, respectively. Recall that d_{ETL}, d_{HTL}, and d_{OLED} are calculated to be 443, 443, and 885 Å in Section 4.3.2 for the green OLED. Thus, this b(t)-v(t)/B-I analysis indicates that the blue ETL is much thicker than the green ETL and the HTLs are approximately the same thickness. This analysis is complicated by the fact that $i^{+}_{offset}(t)$ is not constant for the blue OLED. This may indicate that charge trapping is more significant in blue OLEDs than the green OLEDs.

A b(t)-v(t) curve of the blue OLED is shown in Fig. 4.21. The blue OLED b(t)-v(t) curve has counterclockwise hysteresis, just as the green OLED. Therefore, the blue OLED hysteresis in the b(t)-v(t) curve is also attributed to hole accumulation at the ETL/HTL interface. However, the blue OLED turns on at a much higher voltage than the green OLED and the blue OLED is much dimmer than the green OLED. The shift in turn on of the blue OLED b(t)-v(t) curve to a larger voltage compared to that of the green OLED is most likely due to the thicker ETL of the blue OLED.

A brightness bump could not be observed for the blue OLED. It is unclear if the brightness bump is too small to be detected or if it really is not present. The lack of a prominent brightness bump in the blue OLED may be related the different processing procedures for the fabrication of green and blue OLEDs.

4.5.2 OLEDs Versus PLEDs

Typical i(t)-v(t) curves for an OLED and a PLED are shown in Fig. 4.22. The PLED has a much lower V_t than the OLED and the PLED lacks a current bump. Also, notice that there is a slope to the below-threshold portion of the i(t)-v(t) curve for the PLED, indicating a small R_p. This indicates that the PLED is capable of conducting some leakage charge even at voltages below the threshold voltage. R_s is approximately 58 Ω cm^2 and R_p is approximately 7.7 KΩ cm^2. The bump is absent from the PLED curve because it is a single layer device so that there is no

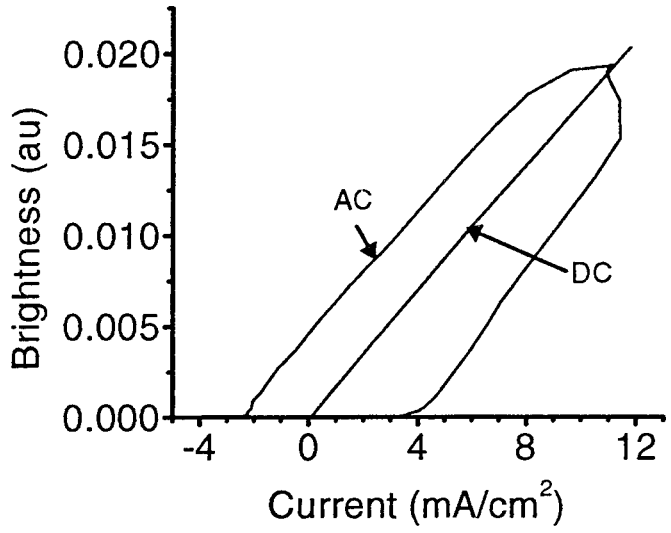

Figure 4.20. A b(t)-v(t)/B-I curve for a blue OLED. Notice that the average value of $i^{+}_{offset}(t)$ is approximately 3.5 mA/cm^2 and $i^{-}_{offset}(t)$ is approximately 2.5 mA/cm^2.

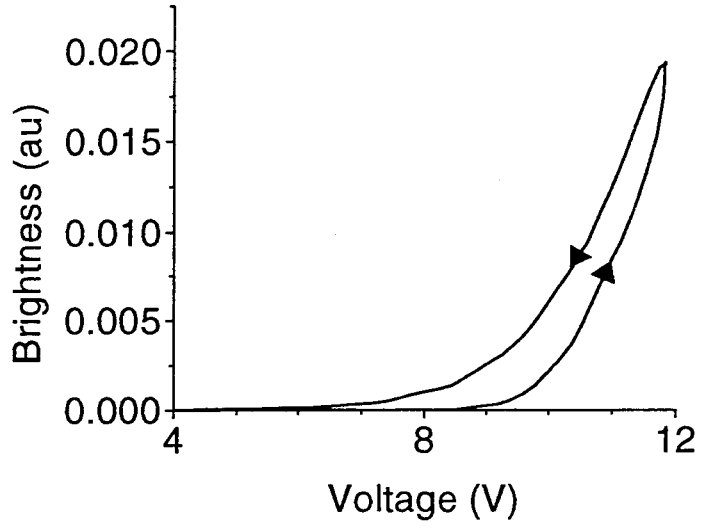

Figure 4.21. A b(t)-v(t) curve for a blue OLED. The curve has counterclockwise hysteresis and turns on at a larger voltage than the green OLED.

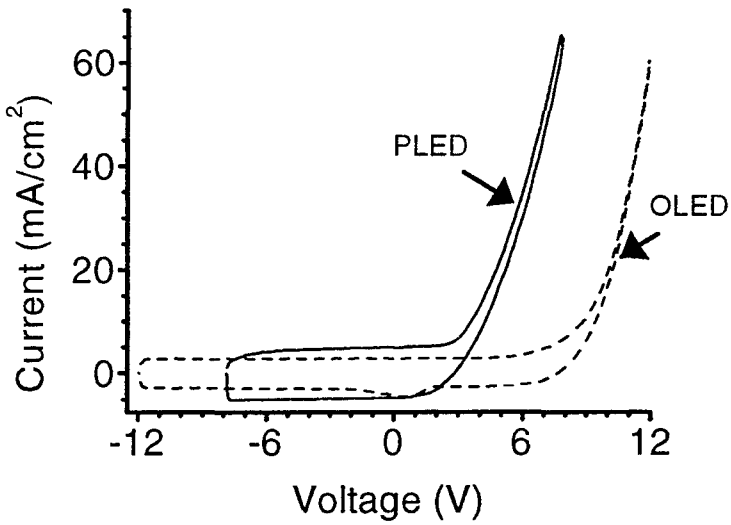

Figure 4.22. i(t)-v(t) curves for a PLED and an OLED. For the PLED i(t)-v(t) curve $V^+_{max} = V^-_{max} = 8$ V. The PLED curve lacks a bump and turns on at a much lower voltage than the OLED. Additionally, the slope of the pre-threshold portion of the PLED i(t)-v(t) curve is non-zero, indicating the existence of a non-infinite shunt resistance.

interface for charge to accumulate. In addition, there cannot be a bump due to charge detrapping because the detrapping charge will not preferentially exit the anode or cathode. Although there are many differences between PLEDs and OLEDs, it is clear that the bump is a result of the heterojuction nature of the OLED. Thus, an i(t)-v(t) bump would be expected for a heterojunction PLED.

The b(t)-i(t)/B-I curves shown in Fig. 4.23 reveal that the PLED behaves similarly to what is expected for a single layer device. $i^+_{offset}(t)$ and $i^-_{offset}(t)$ are approximately equal for most of the applied voltage waveform, indicative of a single layer device. However, $i^+_{offset}(t)$ is larger than $i^-_{offset}(t)$ for large currents. Also, the DC B-I curve is not linear. These offset and nonlinear effects are most likely due to charge trapping and/or leakage of carriers through the PLED (*e.g.* carriers passing through the OLED without recombining). The leakage current my be partially voltage-dependent if the balance of electron and hole injection changes with the ap-

plied bias. $i^{+}_{max} \approx i^{-}_{max} \approx 6$ mA/cm^2 so the total device capacitance is approximately 60 nF/cm^2 and the PLED thickness, d_{PLED} is $\sim$ 590 Å.

Further evidence of charge trapping in PLEDs is revealed by the b(t)-v(t) curve, as shown in Fig. 4.24. The PLED b(t)-v(t) curve has counterclockwise hysteresis and the hysteresis is smaller (*i.e.* $\sim$ 0.1 V and $\sim$ 1 V of hysteresis for PLEDs and OLEDs, respectively) than that of an OLED. With the PLED, the hysteresis is likely due to charge trapping during the rising portion of the applied voltage waveform. As the voltage is ramped up injected carriers are trapped and are unavailable for recombination. However during the downward ramp the traps are full and fewer injected carriers are lost to traps so that more carriers are available for recombination. It is well known that MEH-PPV has many trapping states therefore it is likely that traps have an important role in establishing the hysteretic nature of the b(t)-v(t) curve. [22, 39]

4.5.3 Two Types of Green OLEDs

Throughout most of this thesis work one type of green OLED was investigated. However, another type of green OLED with distinctly different characteristics was obtained near the end of this thesis research. From here on the first green OLED is referred to as type A and the second type of green OLED is denoted type B. Possible reasons for the differences between type A and type B OLEDs are discussed.

Typical type A and B i(t)-v(t) curves are shown in Fig. 4.25. Notice that the type B i(t)-v(t) curve has an increase in the displacement current at about 1.5 V in the positive ramping trace. Also, the current bump is present in type B OLEDs just as in type A OLEDs, although the current bump in type B OLEDs is larger in area. The best explanation for the differences between the two types of OLEDs is that the HTL of the type B OLED can more efficiently transport charge than the HTL of the type A OLED. If holes are injected into and transport through the the type B HTL at a very low forward bias, the HTL becomes conducting at much lower voltages than the ETL. Thus, the increase in the displacement current at about 1.5

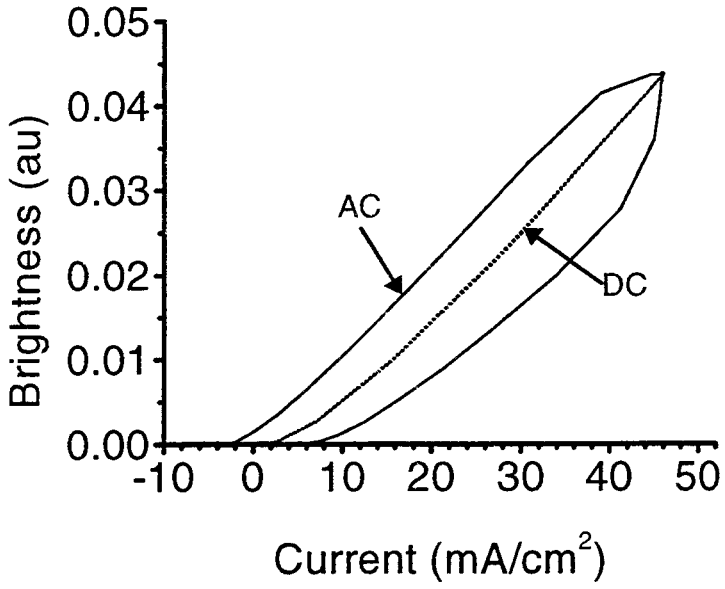

Figure 4.23. b(t)-i(t) and B-I curves for a PLED with $V^+_{max} = V^-_{max} = 3$ V. Notice that $i^+_{offset}(t)$ is approximately equal to $i^-_{offset}(t)$ except for at large currents where $i^+_{offset}(t)$ is larger than $i^-_{offset}(t)$. $i^+_{max} \approx i^-_{offset} \approx 6$ mA/cm^2 for an average value.

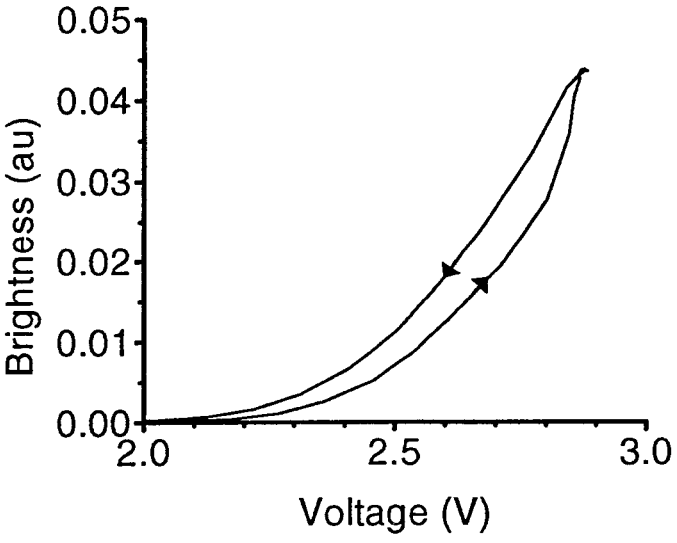

Figure 4.24. A b(t)-v(t) curve for a PLED with $V^+_{max} = V^-_{max} = 3$ V. The b(t)-v(t) curve has counterclockwise hysteresis.

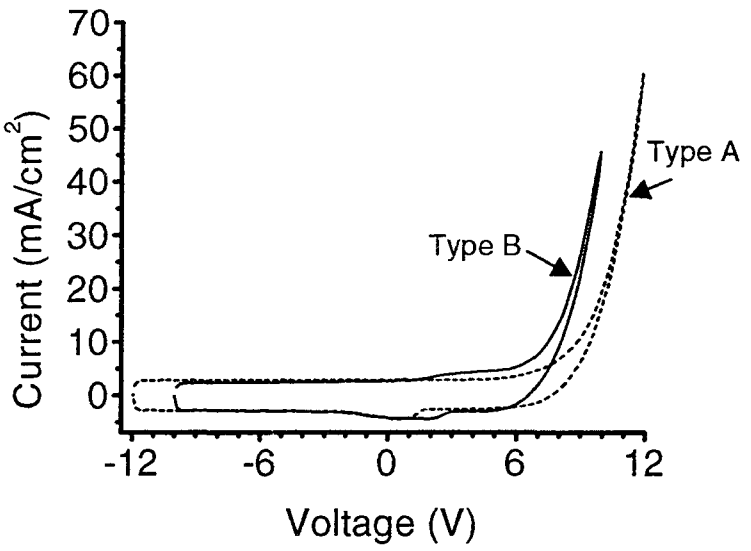

Figure 4.25. i(t)-v(t) curves for a type A and a type B green OLED. $V^{+}_{max} = V^{-}_{max}$ = 10 V for the type B i(t)-v(t) curve. The displacement current of the type B OLED increases near 1.5 V in the positive ramping trace. Also, the area of the current bump is larger for the type B OLED.

V in the type B OLED is caused by the HTL easily conducting charge while the ETL still acts as an insulator. Since the ability of the ETL and HTL to conduct current is grossly mismatched in the type B OLED, the concentration of holes accumulated at the ETL/HTL interface must increase to compensate for this current mismatch. Thus, the current bump is larger in type B OLEDs compared to type A OLEDs.

Typical b(t)-v(t) curves are shown in Fig. 4.26 for type A and B OLEDs. Both type A and type B OLEDs have counterclockwise hysteresis, as expected, since both have significant hole accumulation at the ETL/HTL interface. The type B OLED turns on at a much lower voltage than the type A OLED. This is most likely due to more efficient hole transport in the HTL of the type B OLED. Since hole transport in the type B HTL is more efficient than in the type A HTL, less voltage is dropped across the type B HTL at a given voltage and the type B OLED turns on at a lower voltage.

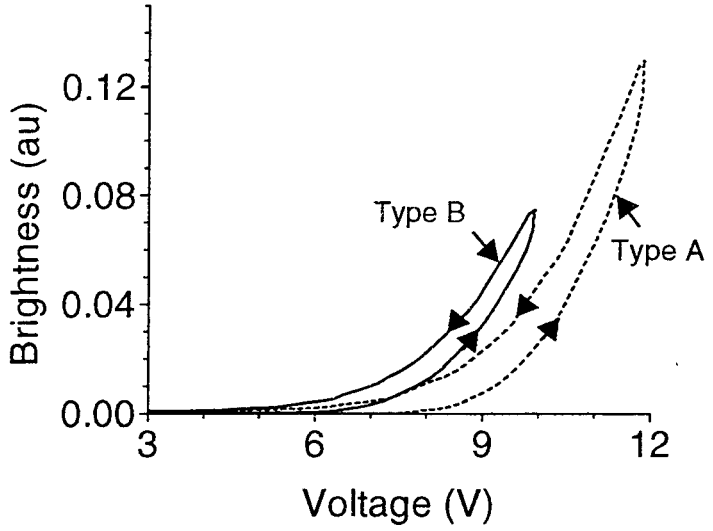

Figure 4.26. b(t)-v(t) curves for type A and type B OLEDs. $V^{+}_{max} = V^{-}_{max} = 10$ V for the type B i(t)-v(t) curve. The type B OLED turns on at a lower voltage than the type A OLED. Both b(t)-v(t) curves have counterclockwise hysteresis.

b(t)-i(t)/B-I curves for a type B OLED are shown in Fig. 4.27. The type B b(t)-i(t) curve is very similar to the type A curve. As with the type A device discussed in Section 4.3.2, d_{ETL}, d_{HTL}, and d_{OLED} may be estimated from b(t)-i(t)/B-I analysis. $i^{+}_{offset}(t)$ and $i^{-}_{offset}(t)$ for the type B OLED are found to be 6 and 4 mA/cm^2, respectively. Assuming a relative permittivity of 4, d_{ETL}, d_{HTL}, and d_{OLED} are estimated to be 590, 295, and 885 Å, respectively. Notice that the displacement currents estimated from the i(t)-v(t) curve of the type B OLED give $\sim$ 3 mA/cm^2 for the total OLED displacement current and $\sim$ 5 mA/cm^2 for the ETL displacement current (*i.e.* the displacement current above $\sim$ 1.5 V). These are slightly smaller than the values estimated from $i^{+}_{offset}(t)$ and $i^{-}_{offset}(t)$. Thus, although there is some uncertainty in this measurement when employed quantitatively, it appears be a useful method for estimating the relative thickness of the ETL and HTL.

A plot of i(t)-v(t) curves for a type B OLED with various V^{+}_{max}'s is shown in Fig. 4.28. The current bump increases in magnitude and then approximately saturates for $V^{+}_{max} \geq 6$ V. Notice that the V^{+}_{max} at which the bump saturates coin-

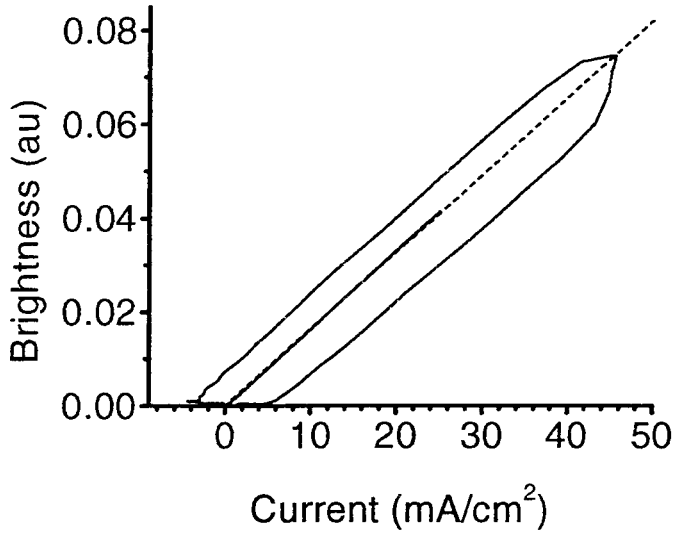

Figure 4.27. b(t)-i(t)/B-I curves of a type B OLED with $V^+_{max} = V^-_{max} = 10$ V. The B-I curve has been extrapolated to larger current as indicated by the dotted line. $i^+_{offset}(t)$ and $i^-_{offset}(t)$ are 6 and 4 mA/cm^2, respectively.

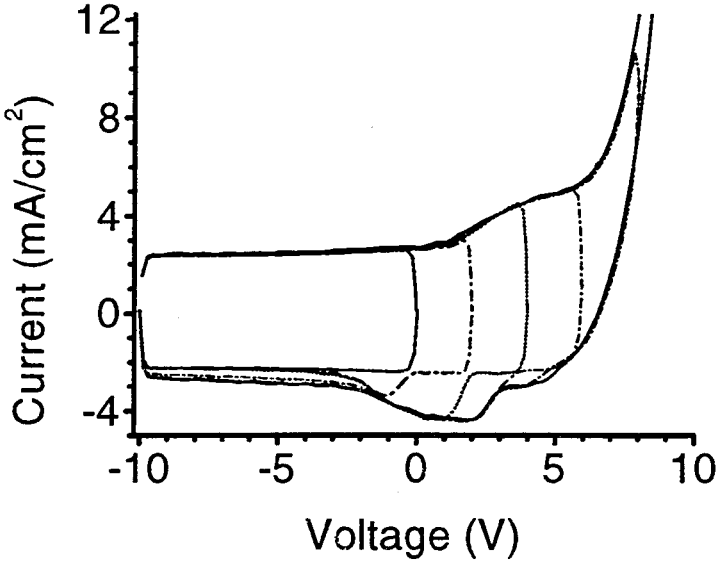

Figure 4.28. i(t)-v(t) curves with $V^-_{max} = 10$ V and $V^+_{max} = 0$, 2, 4, 6, 8, and 10 V, respectively. Notice that the bump saturates for $V^+_{max} \geq 6$ V and saturation of the bump occurs only at V^+_{max}'s large enough for appreciable conduction current to flow.

cides with the V^+_{max} at which the OLED begins to efficiently conduct an appreciable amount of conduction current. The rate-limiting step for efficient OLED current flow is associated with when the ETL is able to transport electrons. Thus, the current bump saturates when the ETL begins to conduct efficiently, as discussed with regard to type A OLEDs in Section 4.3.1. Also, the forward bias characteristics do not change significantly with the type B OLED as V^+_{max} is increased (*e.g.* the type B OLED does not turn on harder with increasing V^+_{max}, see Fig. 4.28). Recall that the type A OLED turns on harder as V^+_{max} is increased, as shown in Fig. 4.4. The type B OLED does not turn on harder with increasing V^+_{max} because the HTL conducts current so much more efficiently than the ETL so that hole accumulation at the ETL/HTL interface occurs in an essentially steady-state manner. In contrast, in the type A OLED the HTL is only slightly more conductive than the ETL so that it is more difficult to accumulate holes at the ETL/HTL interface. Thus, if the ETL is thought of as a capacitor and the HTL a resistor, the RC time constant of the type A OLED is larger than the RC time constant of the type B OLED such that hole accumulation occurs in a non-steady-state and steady-state manner for the type A and B OLEDs, respectively.

At first glance it would appear that the type B OLED would exhibit better performance than the type A OLED due to the improved HTL. This is not necessarily the case, however. In an OLED it is important to maintain charge injection balance within the ETL to insure that most of the injected carriers are annihilated via electron-hole pair recombination. If there are significantly more holes being injected into the ETL than electrons, the holes may travel across the ETL and exit through the cathode as wasted current. Only so many holes can accumulate at the ETL/HTL interface before a significant number of these holes get injected into ETL, transport across the ETL, and exit through the cathode.

4.6 Conclusions

Although many of the results discussed in this chapter are qualitative in nature it is clear that the characterization methods developed in this thesis are of utility for OLED/PLED device physics assessment. Hole accumulation at the ETL/HTL interface is shown to enhance conduction and radiative recombination by increasing the field within the ETL relative to the HTL. The current bump in the i(t)-v(t) curve provides direct experimental evidence that holes accumulate at the ETL/HTL interface. Hole accumulation at the ETH/HTL interface has been previously suggested, but never directly observed. The ETL is shown to behave as a leaky insulator while the HTL more efficiently conducts charge, suggesting that OLED improvements may be obtained by improving injection into and possibly conduction through the ETL. From b(t)-i(t)/B-I analysis, the capacitance and thickness of the ETL and the HTL may be approximated; a summary of the ETL, HTL, and total OLED thicknesses for the devices studied in this thesis are collected in Table 4.1.

Table 4.1. A summary of the thicknesses of the ETL, HTL, and total OLED as estimated from b(t)-i(t)/B-I analysis assuming a relative permittivity of 4. The OLED device area is 0.1 cm^2.

	d_{ETL} (Å)	d_{HTL} (Å)	d_{OLED} (Å)
Green OLED (Type A)	443	443	885
Green OLED (Type B)	531	266	797
Blue OLED	910	364	1274
PLED	-	-	590

Many device parameters are obtained from the methods developed in this thesis, as summarized in Table 4.2. The results obtained from the methods developed in

Table 4.2. A summary of the three primary characterization methods developed in this thesis and the kind of device physics information provided by each.

i(t)-v(t)	b(t)-v(t)	b(t)-i(t)/B-I
C_t	$i^c_{ETL}(t)$ hysteresis	d_{OLED}
current bump	brightness bump	d_{ETL}
V_I		d_{HTL}
R_s		trapping (qualitative)
R_p		
harder/softer turn on with changes in the applied voltage waveform parameters	harder/softer turn on with changes in the applied voltage waveform parameters	

this chapter lead to an improved understanding of OLED operation and increase the number of tools available for OLED characterization.

Chapter 5
Aging Results

In this chapter the results of some preliminary OLED aging experiments are presented. The primary purpose of this chapter is to demonstrate the utility of the OLED analysis methods developed in this thesis. Aging trends are interpreted in terms of the OLED model discussed in Chapter 4.

5.1 Aging of a Green, Type A OLED

A green, type A OLED is aged using the following waveform parameters: an average current density of 20 mA/cm^2, a -15 V reverse voltage pulse amplitude, a 50% on and 50% off waveform, and a frequency of 60 Hz. The aging trends of the forward bias portions of i(t)-v(t) curves are shown in Fig. 5.1. The OLED turns on softer as the OLED is aged and most aging occurs within the first 40 hours of aging. There are two well known sources of OLED aging: (1) degradation of the OLED organic layers, and (2) degradation of the contact metals. Dead areas are observed visually as small, growing dark spots during the operation of the OLED. These dead areas could be caused by either aging mechanism. It is quite possible that both aging mechanisms are operative as the OLED is aged.

Figure 5.2 shows the current bump portions of i(t)-v(t) curves at various aging times. Notice that the area of the current bump decreases as the OLED is aged. However, the voltage at which the current bump initiates, V_I, is approximately constant. This reduction in the area of the current bump may indicate that the HTL/anode and/or ETL/cathode is becoming less conductive. It is also possible to explain the reduction of area of the current bump with aging by a simple loss of effective OLED area (*e.g.* the growth of dark spots in the OLED).

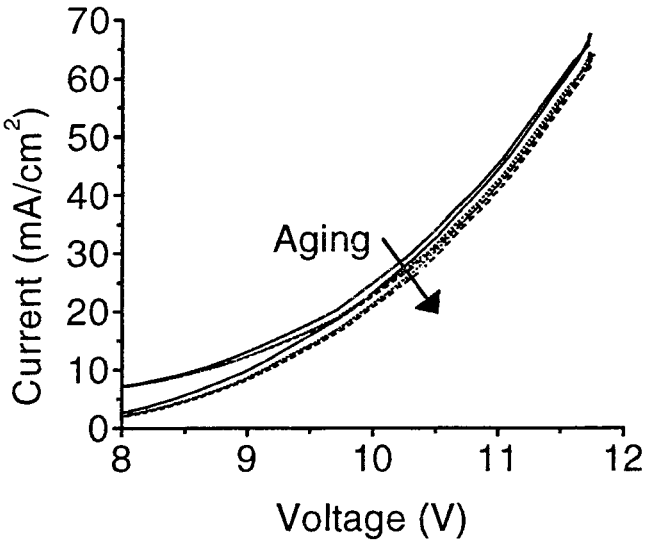

Figure 5.1. The forward bias portion of i(t)-v(t) curves obtained at 0, 40, and 120 hours of aging for a green, type A OLED. Notice that the OLED turns on softer as it is aged and that most of the aging occurs in the first 40 hours.

Notice that the small shift in the displacement current along the current axis in the i(t)-v(t) curve for the 120 hour aged curve, as shown in Fig. 5.2, is likely due to oscilloscope offset. Changes in ambient temperature can cause the offset of the oscilloscope to drift over the 5 day aging period. This problem should be corrected for in future aging studies by either controlling the ambient temperature or by recalibrating the oscilloscope just prior to acquiring data.

As expected, the OLED brightness reduces with aging, as shown in the b(t)-v(t) curves of Fig. 5.3. This reduction in brightness with aging is not exclusively due to the reduction in current; the proportionality between current and brightness, α, also decreases, as shown in Fig. 5.4. The change in α with aging may be due to the growth of dark spots. Dark spots appear to still conduct current, as witnessed by the fact that current is only slightly reduced with aging, but they do not emit light. Thus, the growth of these dark spots reduces the overall OLED efficiency, consistent with the trends in α implicit in Fig. 5.3.

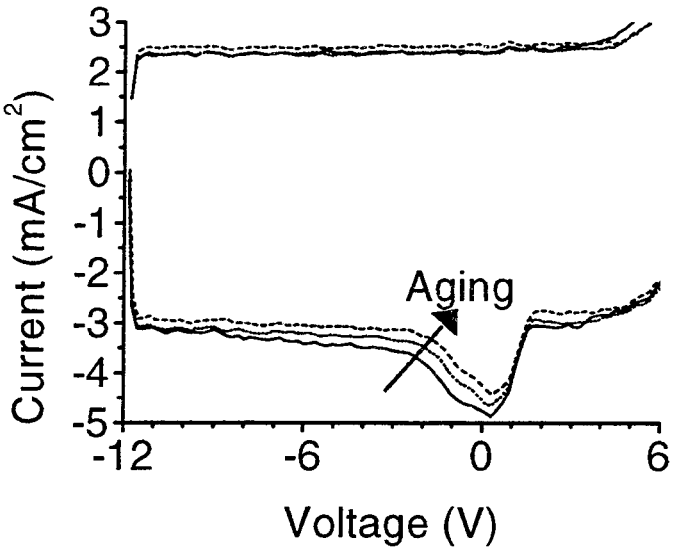

Figure 5.2. The bump portion of i(t)-v(t) curves obtained at 0, 40, and 120 hours of aging for a green, type A OLED. Notice that the area of the current bump decreases as the OLED is aged and V_I remains approximately constant. Also, the offset of the 120 hour aged i(t)-v(t) curve is an artifact of the experiment due to an uncorrected offset of the oscilloscope.

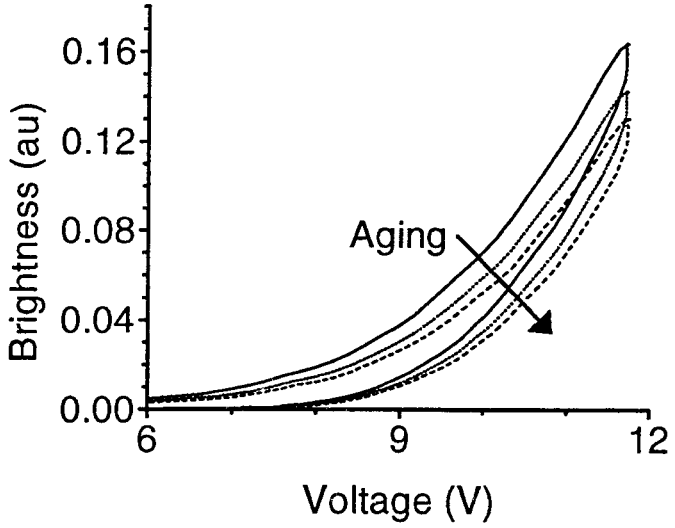

Figure 5.3. b(t)-v(t) curves at 0, 40, and 120 hours of aging for a green, type A OLED. The brightness decreases with aging.

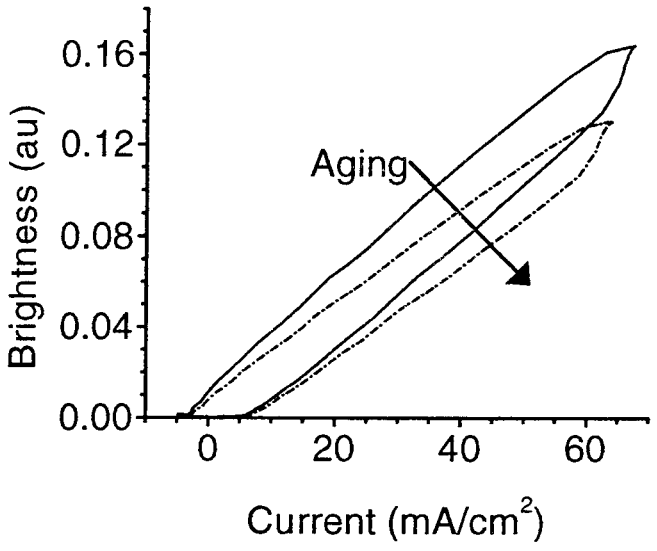

Figure 5.4. b(t)-i(t) curves at 0 and 120 hours of aging for a green, type A OLED. Notice that the proportionality between brightness and current decreases as the OLED is aged.

5.2 Aging of a Green, Type B OLED

A green, type B OLED is aged using the following waveform parameters: average current density of 20 mA/cm^2, a -10 V reverse voltage pulse, a 50% on and 50% off waveform, and a frequency of 60 Hz. The type B OLED ages in a very different manner than the type A OLED. The forward bias i(t)-v(t) curves for the type B OLED actually turn on harder as the OLED is aged, as shown in Fig. 5.5. This trend is difficult explain. It is possible that the ETL conducts charge more efficiently with aging. This explanation seems implausible, as aging unusually causes a layer to become less conductive due to chemical degradation. Alternatively, it is possible that changes in the interface state densities at the anode and/or cathode reduce the barrier height for the injection of holes or electrons, respectively.

The current bump portion of the i(t)-v(t) curve is shown in Fig. 5.6. Notice that the displacement current decreases as the OLED is aged. This is most likely caused by the growth of dark spots on the OLED, effectively reducing the OLED area. The

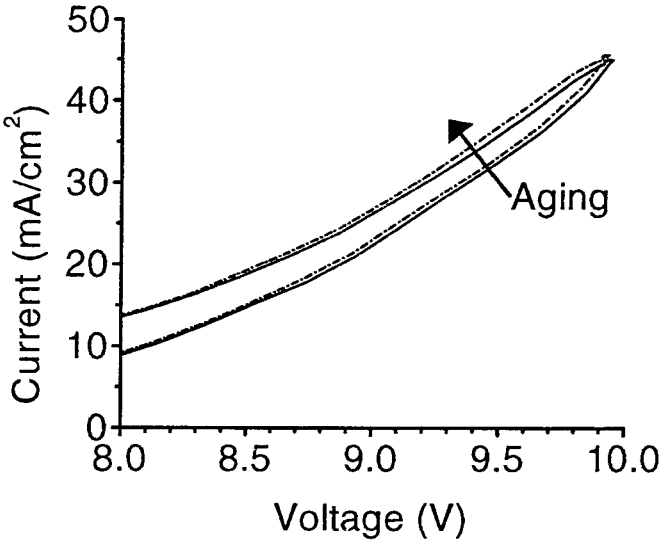

Figure 5.5. The forward bias portion of i(t)-v(t) curves for 0 and 120 hours of aging of a green, type B OLED with $V^+_{max} = V^+_{max} = 10$ V. Notice that the OLED turns on harder as it is aged.

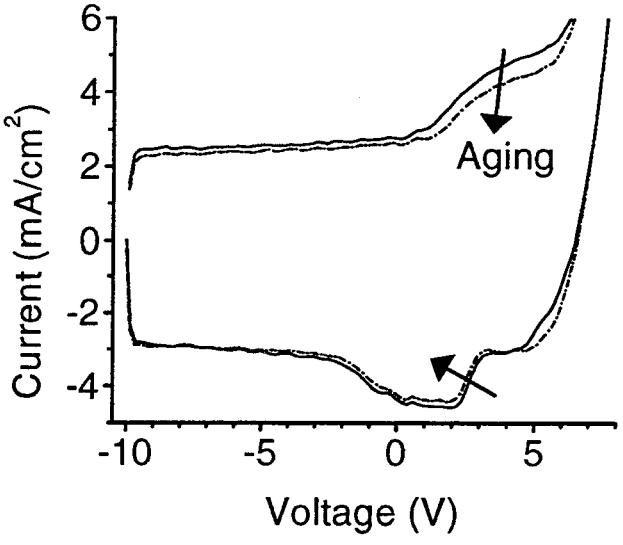

Figure 5.6. The current bump portion of i(t)-v(t) curves for 0 and 120 hours of aging for a green, type B OLED with $V^+_{max} = V^+_{max} = 10$ V. Notice that the displacement current and area of the current bump decrease as the OLED is aged.

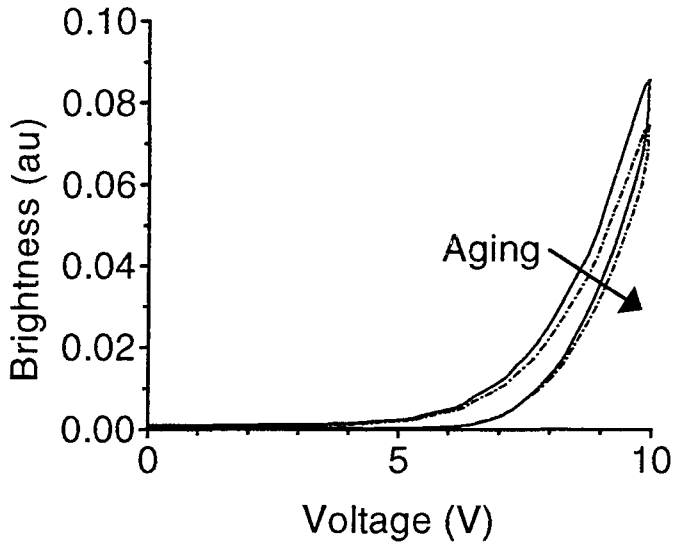

Figure 5.7. b(t)-v(t) curves for 0 and 120 hours of aging for a green, type B OLED with $V^{+}_{max} = V^{+}_{max} = 10$ V. The b(t)-v(t) curves turn on softer as the OLED is aged.

area of the current bump also decreases as the OLED is aged. A reduced OLED area results in less charge accumulation at the ETL/HTL interface and a decrease in the current bump area.

Even though the current turns on harder as the type B OLED ages, the brightness still decreases with aging, as shown in Fig. 5.7. Notice that α decreases as the OLED is aged, as shown in Fig. 5.8. This is a common trend observed in all the aging studies performed in the course of this thesis. It is very likely due to a degradation mechanism involving the incorporation of moisture into the OLED.

5.3 Recovery of an Aged Green, Type A OLED

Previous experiments by D. Zou *et al.* have shown that OLEDs partially recover from aging if the OLED is subjected to a zero or reverse bias for a period of time. [18] In the present aging study, a type A OLED is subjected to a 20 mA/cm^2 DC bias for 120 hours, during which time AC experiments are periodically performed. Approximately one week after the aging cycle, AC data is taken again. During this

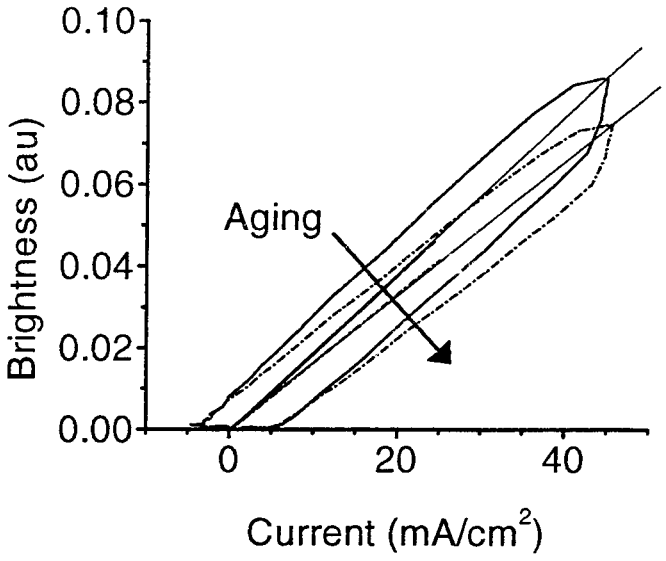

Figure 5.8. b(t)-i(t) and B-I curves for 0 and 120 hours of aging for a green, type B OLED with $V^+_{max} = V^+_{max} = 10$ V. The B-I curves have been extrapolated to large currents. The proportionality between current and brightness decreases as the OLED is aged.

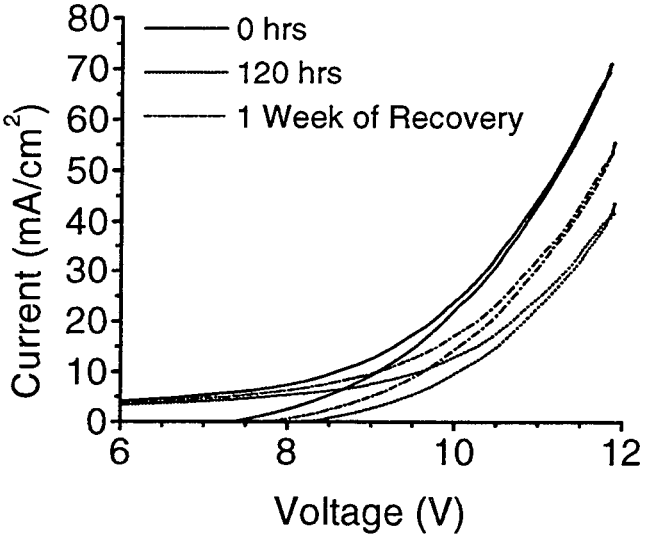

Figure 5.9. The forward bias portion of i(t)-v(t) curves for 0 and, 120 hours of aging, and for 1 week of recovery for a green, type A OLED. Notice that the recovered i(t)-v(t) curve turns on harder than the 120 hour aged curve.

recovery time the OLED was not subjected to any bias. Figure 5.9 shows forward bias i(t)-v(t) curves as the OLED is aged and after it is allowed to recover for 1 week. The forward bias portion of the i(t)-v(t) curve improves dramatically (*i.e.* it turns on harder) when the OLED is given a week of recovery time.

D. Zou *et al.* ascribe this recovery to the movement of ionic impurities within the OLED. [18] These impurities are proposed to move within the OLED in such a way to oppose the applied electric field during forward bias operation. Another possibility is that carriers in deep traps are released during recovery. [3] A large buildup of trapped carriers within the OLED would inhibit current transport. The removal of deeply trapped charge during recovery would improve current transport.

As shown in Fig. 5.10, the current bump shifts toward more negative voltages as the OLED is allowed to recover. V_I of the current bump at 120 hours of aging is roughly 0.5 V more positive than V_I for the recovered curve. Notice that the current bump shifts to more negative voltages by nearly the same amount that the forward bias portion of the i(t)-v(t) curves shift with recovery. This is strong evidence that recovery causes a change in the internal field of the OLED.

The b(t)-v(t) curves do not exhibit a similar recovery trend, as shown in Fig 5.11. The b(t)-v(t) curve turns on softer as the OLED recovers. This is likely due to the fact that the OLED continues to undergo some sort of irreversible aging as the OLED is allowed to recover. This is evidence of some kind of degradation that decreases α, as shown in Fig. 5.12. Degradation of this type is not proportional to current, but rather is associated with chemical degradation of the organic layers, by a process such as oxidation that continues even when no voltage is applied to the OLED. However, this aging mechanism appears to be initiated and sped up by the application of a forward bias since it is possible to store OLEDs in a dry box for long periods of time (2 years) and still have them to operate.

The recovery experiment discussed in this section provides insight into why it is beneficial to operate an OLED with a bipolar waveform. The negative or reverse bias portion of the applied voltage waveform may allow time for the OLED to recover during aging. This negative bias portion may remove deeply trapped charge

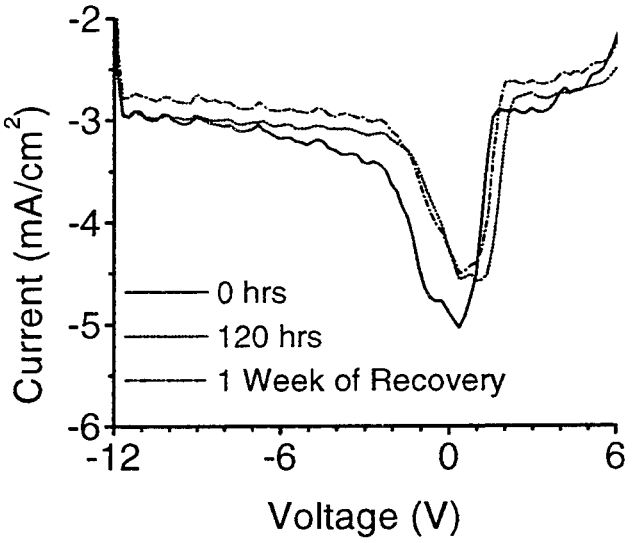

Figure 5.10. The current bump portion of i(t)-v(t) curves for 0 hours and 120 hours of aging, and for 1 week of recovery for a green, type A OLED. Notice that V_I of the recovered curve is shifted approximately 0.5 V more negative than V_I of the 120 hour aged curve.

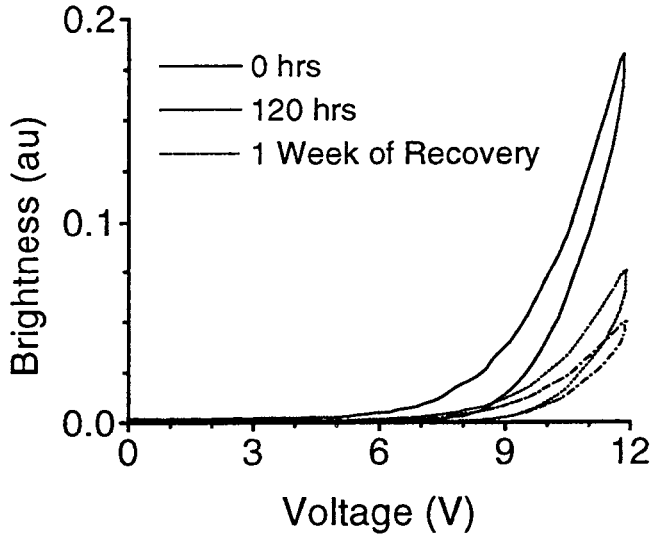

Figure 5.11. b(t)-v(t) curves for 0 and 120 hours of aging, and for 1 week of recovery for a green, type A OLED. Notice that the b(t)-v(t) curve turns on softer after 1 week of recovery.

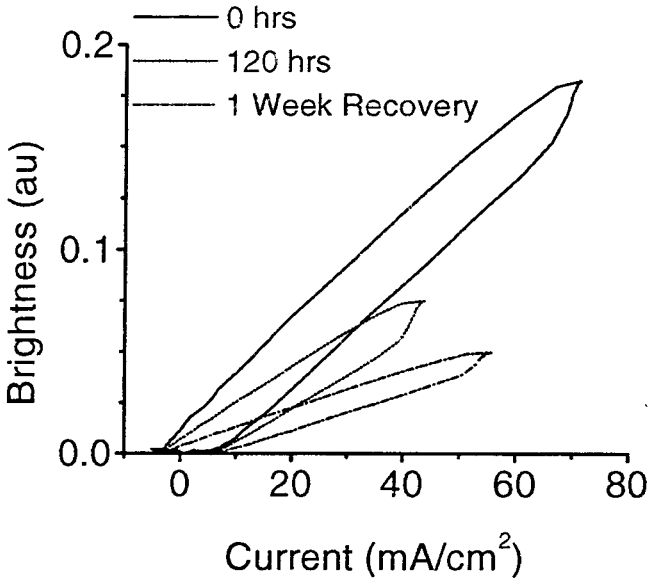

Figure 5.12. b(i)-i(t) curves for 0 and 120 hours of aging, and for 1 week of recovery for a green, type A OLED. Notice that the b(t)-i(t) curve for 1 week of recovery time does not recover and the proportionality between current and brightness is smaller. Also, note that a $i^{+}_{offset}(t)$ and $i^{-}_{offset}(t)$ do not change as the OLED is aged and allowed to recover.

and/or cause the movement of ionic impurities. [3, 18] However, it is unlikely that current due to the movement of ionic impurities or current due to detrapping of deeply trapped charge (*e.g.* trapped charge responsible for reversible aging) could be observed with i(t)-v(t) analysis. The time required for ionic impurities and/or this charge detrapping to occur is likely extremely large ($\sim$ 1 week). Therefore, the current associated with this movement of charge would be excessively small.

5.4 Conclusions

The analysis methods developed in this thesis are shown to be very helpful in elucidating the aging mechanisms of OLEDs. Although much more work needs to be done using these analysis methods, it is clear that they provide much more device physics information than that available by simply monitoring the DC I-V and B-V curves as a function of aging. The analysis methods developed in this thesis have the

ability to monitor the decrease of the effective area of the OLEDs, monitor changes in V_I, monitor changes in the forward bias i(t)-v(t) characteristics and to qualitatively observe changes in the internal OLED field. Also, monitoring changes in α as an OLED is aged allows for quick and easy estimation of the changes in OLED quantum efficiency.

Chapter 6
Conclusions and Recommendations for Future Work

In this thesis many novel experimental methods are developed for OLED characterization. These methods are shown to be very useful in helping to provide an understanding of the physics of OLED operation and are much more informative than simple I-V and B-V plots. Although this work was hindered by not knowing the actual device structure of most of the OLEDs tested, it is clear that a better understanding of OLED performance is obtained by using the characterization methods developed in this thesis.

6.1 Novel Analysis Methods

1. Steady-state transient current-transient voltage [i(t)-v(t)] analysis is introduced as a novel OLED analysis method. From i(t)-v(t) analysis the following OLED parameters may be obtained: OLED capacitance, detrapped charge (*i.e.* the total charge accumulated within the OLED), the voltage at which the current bump initiates (V_I), and qualitative assessment of hard or soft turn on of the OLED. The most important aspect of the i(t)-v(t) analysis method is the current bump. Changes in the current bump relate to changes in the charge stored within the OLED at the ETL/HTL interface and in traps.

2. Steady-state transient brightness-transient current [b(t)-i(t)] analysis is also a novel analysis method developed in this thesis. b(t)-i(t) analysis allows the assessment of the nonradiative current components (*i.e.* the displacement and trapping currents) of the instantaneous current [i(t)]. This analysis method allows the ETL and OLED capacitance to be estimated and therefore the ETL thickness, HTL thickness, and OLED thickness, assuming that conduction current and brightness

are linearly related by a known ratio. b(t)-i(t) analysis also has the potential to provide qualitative information about how the trapping current changes as the applied voltage is ramped. Finally, assessment of the proportionality constant between brightness and current, α, provides a quick and simple method of approximating changes in quantum efficiency with aging.

3. Steady-state transient brightness-transient voltage [b(t)-v(t)] analysis is a novel method introduced in this thesis. The b(t)-v(t) curve is proportional to a ETL conduction current-voltage [i^c_{ETL}(t)-v(t)] curve, assuming that the ETL conduction current and brightness are linearly related. The counterclockwise hysteresis of the b(t)-v(t) curve indicates that accumulation of holes at the ETL/HTL interface increases the ETL conduction current.

4. Steady-state transient current [i(t)] and transient brightness [b(t)] analysis are novel analysis methods introduced in this thesis. The i(t) and b(t) transient curves allow time-dependent features to be observed that cannot be seen in parametric plots. i(t) is dominated by conduction current at large V^+_{max}'s and by displacement and trapping current at low V^+_{max}'s.

5. Detrapped charge analysis is a novel analysis method developed in this thesis. With detrapped charge analysis the transferred charge ($Q_{transferred}$) and the detrapped charge ($Q_{detrapped}$) are calculated and $Q_{detrapped}$-$Q_{transferred}$ and $Q_{detrapped}$-PW^+ curves are generated. From $Q_{detrapped}$-$Q_{transferred}$ curves, it is shown that charge initially injected into the OLED is accumulated at the ETL/HTL interface or is trapped. From a $Q_{detrapped}$-PW^+ curve, it is shown that charge accumulates at the ETL/HTL interface and is trapped during the initial part of the positive bias portion of the applied voltage waveform.

6.2 OLED Comparisons and Device Physics Summary

Use of the analysis methods developed is this thesis provides a methodology for electro-optic characterization of OLEDs. The utility of these characterization methods is demonstrated by employing them to compare and contrast two types of green OLEDs, PLEDs, and blue OLEDs. It is found by comparing PLEDs and OLEDs that the presence of the current bump in i(t)-v(t) curve is only present in hetrojunction devices (*i.e.* OLEDs). Comparison of two types of green OLEDs (Type A and B) and blue OLEDs using the characterization methods developed in thesis demonstrate that differences in device ETL and HTL thickness and material may be distinguished with very little prior knowledge of the OLED structure.

Using the characterization methods developed in this thesis, two important OLED device physics conclusions are obtained: (1) Hole accumulation at the ETL / HTL interface plays an important role in establishing balanced charge injection of electrons and holes into the OLED. (2) The ETL behaves as a leaky insulator while the HTL more efficiently conducts charge and acts as a voltage-dependent resistor.

6.3 Aging

The potential of these analysis methods is demonstrated by testing OLEDs during aging. It is found that aging is characterized by a softer i(t)-v(t) and b(t)-i(t) turn on, a decrease in α, and by the growth of dead spots on the OLED. These dead spots are most likely caused by oxidation of the organic layers and/or metal contacts. Some aging-induced changes are partially recoverable if the OLED is subjected to a long duration zero bias or a reverse bias.

6.4 Recommendations for Future Work

1. Lack of knowledge of the structure of most of the OLEDs test in this thesis seriously inhibited accomplishing a rigorous assessment of the novel OLED characterization methods introduced in this thesis. In future work, the analysis methods

developed in this thesis should be employed to characterize OLEDs of known and varying structure. A more complete understanding of the device structure would aid in verifying the viability of the novel methods developed in this thesis. It would be especially useful to perform b(t)-i(t)/B-I analysis on OLEDs of known structure to determine the accuracy of this analysis method in determining ETL, HTL, and OLED thicknesses.

2. A computer-based device physics model should be developed to simulate OLED behavior when subjected to the analysis methods developed in this thesis. Only when accurate models are able to simulate the behavior of OLEDs under a variety of experimental conditions will the full potential of the characterization methods developed in this thesis be realized. With an accurate computer model it will be possible to make predictions about how to improve OLED efficiency and reliability.

3. One aging trend observed in the OLEDs tested in this thesis was the growth of dark spots. These dark spots are thought to be related to moisture contamination. Many of the OLEDs tested in this thesis had very poor encapsulation; it is essential that this problem be corrected in commercial products. Also, reliable aging studies providing insight into the fundamental OLED degradation mechanisms can only be accomplished when the OLED is properly encapsulated so that the incorporation of moisture is not a factor.

4. Drift in the oscilloscope offset sometimes resulted in questionable aging results. Two possible ways of correcting for oscilloscope offset may be to carefully maintain the ambient temperature during an aging study or to calibrate the oscilloscope prior to each measurement during the aging cycle. This offset problem should be addressed before further aging studies are undertaken.

5. Studies comparing and contrasting aging with various waveforms using the novel characterization methods developed in this thesis should be undertaken. It is known that the reverse bias period of an applied voltage waveform improves the aging

characteristics. However, exactly why, how much, and how long the reverse bias should be applied is not known. A more complete understanding of reversible aging trends may allow better OLED driving waveforms to be developed.

BIBLIOGRAPHY

[1] C. W. Tang and S. A. VanSlyke, "Organic electroluminescent diodes," *Appl. Phys. Lett.*, vol. 51, pp. 913–15, Sept. 1987.

[2] C. W. Tang, S. A. VanSlyke, and C. H. Chen, "Electroluminescence of doped organic thin films," *J. Appl. Phys.*, vol. 65, pp. 3610–16, May 1989.

[3] S. A. VanSlyke, C. H. Chen, and C. W. Tang, "Organic electroluminescent devices with improved stability," *Appl. Phys. Lett.*, vol. 59. pp. 2160–62, Oct. 1996.

[4] I. D. Parker, "Carrier tunneling and device characterization in light-emitting diodes," *J. Appl. Phys.*, vol. 75, pp. 1656–66, Feb. 1993.

[5] J. C. Carter, I. Grizzi, S. K. Heeks, D. J. Lacey, S. G. Latham, P. G. May, O. Ruiz de los Panos, K. Pichler, C. R. Towns, and H. F. Wittmann, "Operating stability of light-emitting polymer diodes based on poly(p-phenylene vinylene)," *Appl. Phys. Lett.*, vol. 71, pp. 34–36, July 1997.

[6] S. Berleb, W. Brutting, M. Schwoerer, R. Wehrmann, and A. Elschner, "Effects of majority carrier space charges on minority carrier injection in dye doped polymer light-emitting devices," *J. Appl. Phys.*, vol. 83, pp. 4403–09, Jan. 1998.

[7] E. N. Kaufmann, ed., *Annual Review of Materials Science*, vol. 27, ch. Electrical Characterization of Thin-Film Electroluminescent Devices, pp. 223–248. Palo Alto: Annual Reviews Inc., 1997.

[8] P. E. Burrows, Z. Shen, V. Bulovic, D. M. McCarty, and S. R. Forrest, "Relationship between electroluminescene and current transport in organic heterojunction light-emitting devices," *J. Appl. Phys.*, vol. 79, pp. 7991–8006, May 1996.

[9] R. G. Kepler, P. M. Beeson, S. J. Jacobs, R. A. Anderson, M. B. Sinclair, V. S. Valencie, and P. A. Cahill, "Electron and hole mobility in tris(8 - hydrox-

yquinolinolato - N1,O8) aluminum," *Appl. Phys. Lett.*, vol. 66, pp. 3618–20, June 1995.

[10] C. Hosokawa, H. Tokailin, H. Higashi, and T. Kusumoto, "Transient behavior of organic thin film electroluminescence," *Appl. Phys. Lett.*, vol. 60, pp. 1220–22, Mar. 1992.

[11] K. C. Kao and W. Hwang, *Electrical Transport in Solids*, vol. 14. New York: Pergamon Press, 1981.

[12] M. Pope and C. E. Swenberg, *Electronic Processes in Organic Crystals.* New York: Clarendon Press, 1982.

[13] F. Gutmann and L. E. Lyons, *Organic Semiconductors Part A.* Malabar, Florida: Robert E. Krieger Publishing Company, 1981.

[14] F. Gutmann, H. Keyzer, L. E. Lyons, and R. B. Somoano, *Organic Semiconductors Part B.* Malabar, Florida: Robert E. Krieger Publishing Company, 1983.

[15] C. W. Tang, "An overview of organic electroluminescent materials and devices," *J. of the SID*, vol. 5, no. 1, pp. 11–14, 1997.

[16] J. F. Wager, W. Barrow, and P. Green, "Oled discussion." Private Communication, May 1997.

[17] M. Matsumura and Y. Jinde, "Voltage dependance of light-emitting zone in aluminum-hydroxyquinoline layers of organic heterojunction el devices," *IEEE Trans. Electron Devices*, vol. 44, pp. 1229–33, Aug. 1997.

[18] D. Zou, M. Yahiro, and T. Tsutsui, "Effects of reverse-bias on device performance in organic light emitting diodes," *J. of the SID*, 1998. in press.

[19] P. E. Burrows, V. Bulovic, S. R. Forrest, L. S. Sapochak, D. M. McCarty, and M. E. Thompson, "Reliablity and degradation of organic light emitting devices," *Appl. Phys. Lett.*, vol. 65, pp. 2922–24, Dec. 1994.

[20] H. Aziz, Z. Popovic, C. P. Tripp, N.-X. Hu, A.-M. Hor, and G. Xu, "Degradation processes at the cathode/organic interface in organic light emitting devices with Mg:Ag cathodes," *Appl. Phys. Lett.*, vol. 72, pp. 2642–44, May 1998.

[21] J. R. Sheats, H. Antoniadis, M. Hueschen, W. Leonard, J. Miller, R. Moon, D. Roitman, and A. Stocking, "Organic electroluminescent devices," *Science*, vol. 273, pp. 884–88, Aug. 1996.

[22] P. W. M. Blom, M. J. M. de Jong, and J. J. M. Vleggaar, "Electron and hole transport in ploy(p-phenylene vinylene) devices," *Appl. Phys. Lett.*, vol. 68, pp. 3308–10, June 1996.

[23] E. M. Conwell and M. W. Wu, "Contact injection into polymer light-emitting diodes," *Appl. Phys. Lett.*, vol. 70, pp. 1867–69, Apr. 1997.

[24] M. Matsumura, Y. Jinde, T. Akai, and T. Kimura, "Analysis of current-voltage characteristics of organic electroluminescent devices on the basis of schottky emission mechanism," *Jpn. J. Appl. Phys.*, vol. 35, pp. 5735–39, Aug. 1996.

[25] J. Yang and J. Shen, "Doping effects in organic electroluminescent devices," *J. Appl. Phys.*, vol. 84, pp. 2105–11, May 1998.

[26] J. Shen and J. Yang, "Physical mechanisms in double-carrier trap-charge limited transport processed in organic electroluminescent devices: A numerical study," *J. Appl. Phys.*, vol. 83, pp. 7706–14, Mar. 1998.

[27] J. P. Bender, B. J. Norris, and J. F. Wager, "Oled modeling via spice," *J. of the SID*, 1998. in press.

[28] L. S. Hung, C. W. Tang, and M. G. Mason, "Enhanced electron injection in organic electroluminescence devices using an Al/LiF electrode," *Appl. Phys. Lett.*, vol. 70, pp. 152–54, January 1997.

[29] G. E. Jabbour, Y. Kawabe, S. E. Shaheen, J. F. Wang, M. M. Morrell, and B. Kippelen, "Highly efficient and bright organic electroluminescent devices with an aluminum cathode," *Appl. Phys. Lett.*, vol. 71, pp. 1762–64, September 1997.

[30] G. E. Jabbour, R. Schlaf, N. R. Armstrong, B. Kippelen, and N. Peyghambarian, "Effects of insulating layers on the performance of organic electroluminescent deviecs," *SPIE Proceedings*, 1998. in press.

[31] H. Tang and J. Shinar, "Bright high efficiency blue organic light-emitting diodes with Al_2O_3/Al cathodes," *Appl. Phys. Lett.*, vol. 71, pp. 2560–62, November 1997.

[32] S. Eugusa, N. Germma, A. Miura, K. Mizushima, and M. Azuma, "Carrier injection characteristics of the metal/organic junctions of organic thin-film devices," *J. Appl. Phys.*, vol. 71, pp. 2042–44, February 1992.

[33] S. Eugusa, A. Miura, N. Germma, and M. Azuma, "Carrier injection characteristics of organic electroluminescent devices," *Jpn. J. Appl. Phys.*, vol. 33, pp. 2741–45, February 1994.

[34] D. V. Khramitchenkov, H. Bassler, and V. I. Arkhipov, "A model of electroluminescence in organic double-layer light-emitting diodes," *J. Appl. Phys.*, vol. 79, pp. 9283–9290, June 1996.

[35] D. V. Khramitchenkov, V. I. Arkhipov, and H. Bassler, "Charge carrier recombination in organic bilayer electroluminescent diodes. I. theory," *J. Appl. Phys.*, vol. 81, pp. 6954–6962, May 1997.

[36] J. C. Hitt, J. F. Wager, and B. J. Norris, "Oled circuit model discussion." Private Communication, June 1999.

[37] S. M. Sze, *Physics of Semiconductor Devices.* New York: John Wiley and Sons, second ed., 1981.

[38] V. R. Nikitenko, V. I. Arkhipov, Y. H. Tak, J. Pommerehne, and H. Bassler, "The overshoot effect in transient electroluminescence from organic bilayer light emitting diodes: Experiment and theory," *J. Appl. Phys.*, vol. 81, pp. 7514–25, June 1997.

[39] M. Meier, S. Karg, K. Zuleeg, W. Brutting, and M. Schwoerer, "Determination of trapping parameters in poly(p-phenylenevinylene light-emitting devices using thermally stimulated currents," *J. Appl. Phys.*, vol. 84, pp. 87–92, July 1998.